Mathematical Modeling of Nitrogen-Pressurized Halon Flow in Fire Extinguishing Systems

Aitor Amatriain[a], Gonzalo Rubio[a], Ignacio Parra[a], Eusebio Valero[a], David Andreu[b], Pedro Manuel Martín[b]

[a] *E.T.S. Ingeniería Aeronáutica y del Espacio / Universidad Politécnica de Madrid*
Plaza Cardenal Cisneros, 3, 28040, Madrid, Spain
[b] *Airbus Operations – Power Units Integration*

Abstract

In this work the discharge process of a fire extinguishing agent through a pipe is studied. Particularly, Halon 1301 is considered, an halocarbon that is introduced in bottles pressurized by nitrogen. Nitrogen dissolves in Halon at high pressure, so the bottle contains a multicomponent liquid. Moreover, the discharge process typically entails phase change leading to three different discharge steps with complex governing equations. Therefore the driven forces of each case are analysed and a simplified model is proposed. The results given by the developed model are validated with numerical and experimental data provided by NASA [D.G. Elliott et al. Flow of Nitrogen-Pressurized Halon 1301 in Fire Extinguishing Systems, JPL Publication 84 (1984) [15]], consisting of a discharge of Halon 1301 and nitrogen mixture through a nozzle of reduced length. Finally, numerical results corresponding to a case of practical application are shown, and a parametric study is presented.

Keywords: Halon, Multicomponent mixture, Multiphase flow, Fire extinguishing systems

1. Introduction

The problem of choosing the optimum fire extinguishing system for a specific situation has been widely analysed in the aviation industry [2]. This is because the extinguishing agent has to be selected taking into account several features as effectivity, damage to electronic equipment and toxicity. The prime example are the Halons, chemical compounds that are derived from methane.

Halogenated agents were developed in the late nineteenth century with the first of the agents, Halon 104 [5]. As time has passed, several different Halons have been proposed, specially during World War II. In 1947, Purdue University conducted several tests to study the effectiveness of sixty fire extinguishing agents, most of them Halons, and concluded that the effectiveness in fire extinction properties increases with an increase in molecular weight [25]. Moreover, the number of potential agents was reduced to four: Halon 1201, Halon 1211, Halon 1301 and Halon 2402.

Halon 1301 and 1211 have been by far the most employed Halons, specially nitrogen-pressurized Halon 1301. Developed in a joint venture between the U.S. Army and DuPont in 1954, despite its high cost, it is more effective and less toxic than Halon 1211. Like other Halons, it is not corrosive to modern construction materials, which makes it suitable for sensitive computer and electronics equipment.

However, the 1987 Montreal Protocol represented a turning point for the extinguishing agents, as those that contribute to the ozone depletion, including Halons, started to be banned. Halon production ceased in 1994 [17], but, although several alternatives are under analysis, it is still widely used by the aeronautical industry as fire extinguishing agent [16].

At present, most of the fire extinguishers that are used have been validated by means of experiments. Since the available amount of Halons is reduced, experiments are expensive. In addition, if an important modification is required in the compartments where fire extinguishers are located, it is not simple to predict the adjustments needed to certify new configurations. This is the reason why it is necessary to develop mathematical models capable of predicting the values of the thermodynamic properties at the exit of the system, which often consists of a bottle joined to a pipe.

To the authors knowledge, the first article related to the simulation of Halon discharge was published by NASA [15]. In that work, the authors considered the temporal and spatial evolution of the discharge of a nitrogen-pressurized vessel through a pipe, and three different discharge steps were identified: as a liquid during initial instants, as a two-phase mixture at intermediate times, and finally, as a gas. It was also confirmed that nitrogen dissolves in Halon, so the three fluids are multicomponent. Moreover, an homogeneous model was proposed, whose accuracy is remarkable in the studied experimental cases. Nevertheless, the underlying physics is not considered in detail, as the thermodynamic properties of the model are mainly based on empirical correlations. As a result, there is a high uncertainty in the validity

of that model in different conditions that the ones considered there.

Other studies have been based on analytical models [9] and commercial software [21, 22]. Its accuracy is questionable, since important simplifications are shown in terms of thermodynamics, and no experimental comparison is available. Another noteworthy work has been focused on both mathematical modeling and experimental results [32]. The authors make use of the RELAP solver [14], widely used by the nuclear industry in the analysis of water-steam systems. The extension to halogenated mixtures is done with the aid of REFPROP database [19]. The combination of both programs results in a more robust model than the previous ones, as less correlations are needed. Despite the fact that the obtained results match notably the experimental results, the treatment of liquid and gas mixtures lacks some important features, as saturation properties do not take into account the multicomponent nature of the mixture. In addition, the presence of parameters to adjust the model leads to uncertainty about the applicability in different conditions.

Based on the previous ideas, the main objective of this work is to analyse the main features of the Halon discharge process. This will be done by considering a simple one dimensional model in terms of the geometry, while focusing the efforts in the thermodynamics of multiphase and multicomponent mixtures, an aspect that has not been previously discussed in detail. For that purpose, this work is divided into three sections: first of all, the mathematical model (Section 2) allows to obtain a simplified system of the Navier-Stokes equations; secondly, the results corresponding to numerical simulations are validated and a parametric study is conducted to study the effect of several parameters (Section 3), and, finally, some conclusions are drawn (Section 4).

2. Mathematical model

First of all, Figure 1 shows a representative 3D model of the system that will be studied. It consists of a discharge vessel (light grey), which is joined to a straight pipe (black) by means of a discharge outlet (dark grey). The vessel is filled with a fire supressant, Halon 1301, and then pressurized by adding nitrogen until reaching a pressure around 1-10 MPa. It has to be stressed the existence of a valve between the bottle and the discharge outlet, that prevents the discharge from starting.

The main objective of this section is to propose a one dimensional mathematical model that takes into account the most important features of the

discharge process. This will be done in four parts: first of all, the initial condition of the system is analysed (Section 2.1); secondly, a system of equations is obtained for the discharge process (Section 2.2); then, the numerical implementation of the equations is explained (Section 2.3), and, finally, the main limitations of the model are discussed (Section 2.4).

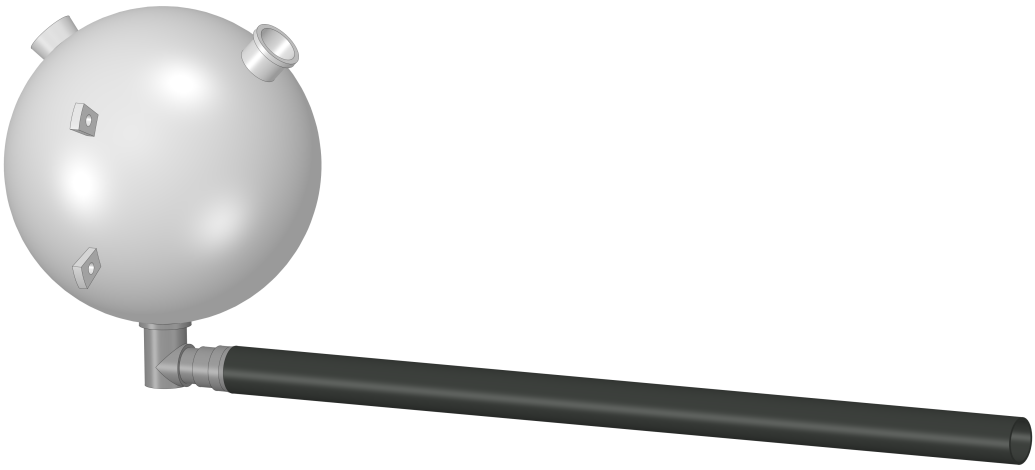

Figure 1: Representative 3D model of the system

2.1. Initial condition

The initial state of the system is sketched in Figure 2. The pressurized vessel contains nitrogen dissolved in Halon, and an amount of evaporated Halon to reach an equilibrium state.

The inputs of the system are: temperature T_0, bottle volume V_b, nitrogen mass m_{n_0} and Halon mass m_{h_0}. Thermodynamic equilibrium at the initial state is assumed, and making use of Peng-Robinson equation of state [27], the values of the following variables are calculated at $t = 0$ (see Appendix B.1): bottle pressure, p_{b_0}, liquid volume, V_{l_0}, liquid and gas densities, ρ_{l_0} and ρ_{g_0} and liquid and gas compositions in mole fractions, $\mathcal{X}_{k_0}$ and $\mathcal{Y}_{k_0}$. This allows to compute the values of all the physical properties (see Appendix C), which are assumed to be constant during the simulation. It is important to stress that the range of temperatures where the model is valid is limited by the critical temperature of the mixture (see Appendix B.4).

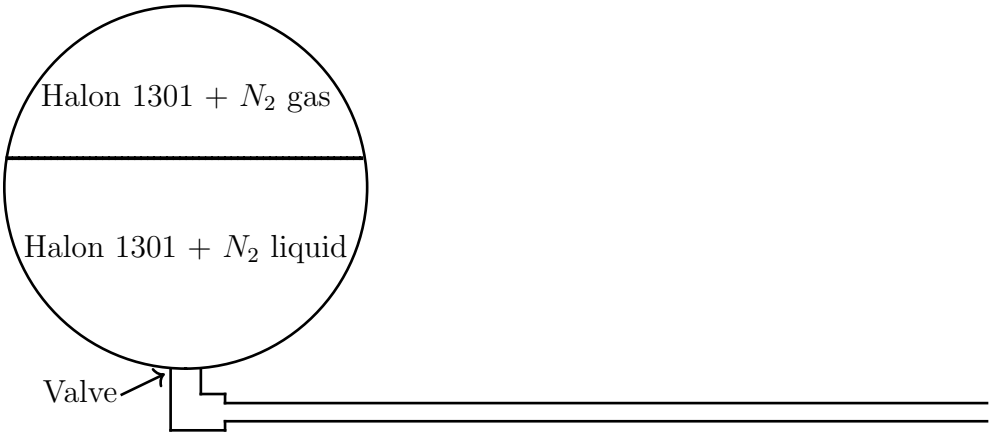

Figure 2: Initial condition of the system

2.2. Discharge

As previously stated, Halon discharge consists of up to three steps. In each one, pipe outlet fluid has different properties:

1. Step 1: Liquid discharge.
2. Step 2: Two-phase mixture discharge.
3. Step 3: Gas discharge.

As a consequence of the above, this section is divided into four parts: Step 1 (Section 2.2.1), Step 2 (Section 2.2.2), Step 3 (Section 2.2.3) and transitions between steps (Section 2.2.4). It has to be noted that all steps share several hypotheses:

- The valve is not present during the discharge, assuming that it is removed mechanically or by means of an explosive.
- Peng-Robinson equation of state is used, as the fluids are multicomponent and $p_{b_0} \gg p_o$, where p_o is sea level standard atmospheric pressure.
- Viscous dissipation and the work made by mass forces are not considered due to the bottle high-pressure constraint.
- Thermal conduction is not taken into account. This is because the characteristic time of thermal conduction is much higher than the characteristic discharge time.

- Stagnation pressure is conserved between the bottle and the discharge outlet, as $Re \gg 1$ in this region and the characteristic length of the discharge outlet is much less than the characteristic length of the bottle.

- The motion in the pipe is stationary, due to the fact that pipe residence time is smaller than bottle residence time.

2.2.1. Step 1. Liquid discharge

Step 1 consists of Halon 1301 and nitrogen discharge in liquid phase. The liquid is in metastable state, and wall cavities or impurities in the bulk of the liquid lead to bubble formation at nucleation sites [12], although surface tension prevents them from growing. Step 1 is finished at $t = t_1$ when bottle pressure equals saturation pressure minus the pressure exerted by bubble surface tension or the bottle runs out of liquid.

A relevant question is if the vapor mass flux J_m extended over the liquid-vapor surface will give rise to modifications in gas composition. To study this possibility, Fick's law gives $J_{m_k} = \rho_g D_k \nabla Y_k \sim \rho_g D_k/\delta$, being δ the width of the mass boundary layer. Taking as reference the values of diffusion coefficients of bromoalkenes in nitrogen [35], then $D_k \sim 10^{-6}$ m^2/s, and $\delta \sim \sqrt{D_k t}$, which is the self-similar variable of a diffusion process. Setting $\rho_g \sim 100$ kg/m^3, discharge time $t_d \sim 1$ s and liquid-vapor surface area $S \sim 10^{-2}$ m^2, then mass transfer $m \sim J_{m_k} S/t_d \sim 0.001$ kg $\ll m_{k_0}$, therefore the change of composition can be neglected in the present model.

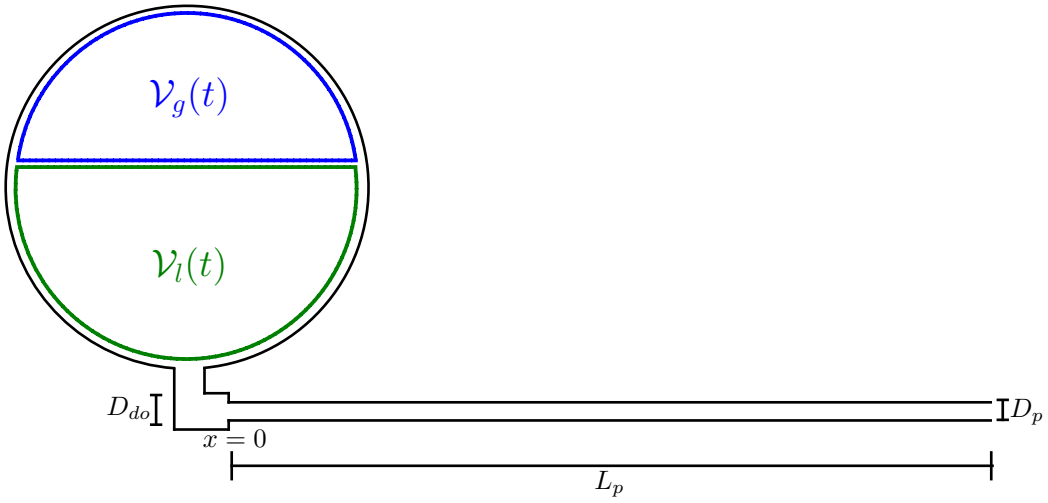

Figure 3: Control volumes corresponding to the system of equations of Step 1

Considering that the liquid is incompressible ($\rho_l = \rho_{l_0}$), together with the fact that the gas is calorically perfect, the system of equations corresponding to Step 1 is presented hereunder. Firstly, a system of ordinary differential equations in the control volumes $\mathcal{V}_g$ and $\mathcal{V}_l$:

$$\begin{cases} \dfrac{\mathrm{d}V_l}{\mathrm{d}t} = -v_{p_0} A_p \quad \text{in } \mathcal{V}_l \times [0, t_1]; & (1) \\ T_l = \dfrac{p_b W_l}{\hat{Z}^l \rho_l R} \quad \text{in } \mathcal{V}_l \times [0, t_1]; & (2) \\ \dfrac{\mathrm{d}\rho_g}{\mathrm{d}t} = -\dfrac{\rho_g v_{p_0} A_p}{V_b - V_l} \quad \text{in } \mathcal{V}_g \times [0, t_1]; & (3) \\ \dfrac{\mathrm{d}T_g}{\mathrm{d}t} = -\dfrac{p_b v_{p_0} A_p}{\rho_g c_v (V_b - V_l)} \quad \text{in } \mathcal{V}_g \times [0, t_1]; & (4) \\ \rho_g = \dfrac{p_b W_g}{\hat{Z}^v R T_g} \quad \text{in } \mathcal{V}_g \times [0, t_1]; & (5) \\ V_l = V_{l_0},\ T_l = T_0 \quad \text{on } \mathcal{V}_l \times \{0\}; & (6) \\ \rho_g = \rho_{g_0},\ T_g = T_0 \quad \text{on } \mathcal{V}_g \times \{0\}. & (7) \end{cases}$$

In the previous equations, V is the volume of the corresponding control volume, v velocity, A area, T temperature, ρ density, p pressure, R ideal gas constant, c_v specific heat at constant volume (see (C.11)), W molecular mass, $\hat{Z}^l$ liquid compressibility factor and $\hat{Z}^v$ gas compressibility factor. Subindexes g, l, p and 0 are referred to gas, liquid, pipe and inlet, respectively.

Secondly, the simplified Navier-Stokes equations for the pipe flow are:

lin

$$\begin{cases} \dfrac{\partial v}{\partial x} = 0 \quad \text{in } [0, L_p] \times [0, t_1]; & (8) \\ \dfrac{\partial p}{\partial x} = -\rho_l \lambda \dfrac{v^2}{2 D_p} \quad \text{in } [0, L_p] \times [0, t_1]; & (9) \\ T = \dfrac{p W_l}{\hat{Z}^l R \rho_l} \quad \text{in } [0, L_p] \times [0, t_1]; & (10) \\ p = p_b - \dfrac{1}{2} \rho_l v_{p_0}^2 \Big(\dfrac{A_p}{A_{do}} \Big)^2 \left\{ \Big(\dfrac{A_{do}}{A_p} \Big)^2 + \lambda \dfrac{L_{do}}{D_{do}} \right\} \text{ and} & \\ v = \dfrac{G}{\rho_l A_p} \quad \text{on } \{0\} \times [0, t_1]; & (11) \\ p = \max(p_{sat}(T, \mathcal{X}) - p_{st}, p_a) \quad \text{on } \{L_p\} \times [0, t_1]. & (12) \end{cases}$$

Variables D and L are diameter and length, where $do \equiv$ discharge outlet, while G is mass flow rate and p pressure, being $a \equiv$ ambient. The parameter p_{st} is the pressure exerted by surface tension:

$$p_{st} = \frac{4\sigma}{D_{bub}}, \tag{13}$$

where σ is Halon 1301 surface tension (see (C.10)) and $D_{bub} = 15 \cdot 10^{-9}$ m bubble nucleation diameter [15].

Furthermore, Darcy-Weisbach equation has been considered for the pressure loss [11]. Assuming $Re_t = 3000$, the friction coefficient λ reads [8]:

$$\begin{cases} \lambda = \dfrac{64}{Re} & \text{if } Re < Re_t \\ \dfrac{1}{\sqrt{\lambda}} = -2\log\left(\dfrac{\varepsilon}{3.7D_p} + \dfrac{2.51}{Re\sqrt{\lambda}}\right) & \text{if } Re \geq Re_t \end{cases} \tag{14}$$

Finally, saturation pressure p_{sat} is computed by means of chemical equilibrium equation, and the value of mass flow rate G is the one which allows to satisfy the boundary conditions for the pressure at $x = 0$ and $x = L_p$.

2.2.2. Step 2. Two phase mixture discharge

In liquids, bubble growth phenomenon is difficult to model, as there are a large amount of nuclei. Initially, each bubble is not affected by the growth of the surrounding ones, but this is not the case as bubble radii increase. Consequently, it is not easy to model this physical process. However, a study of multicomponent bubble growth at high pressure [1] shows that the characteristic time of bubble growth is closely related to the following parameter:

$$\delta = \frac{\dfrac{\rho_g}{\rho_l}}{1 - \dfrac{\rho_g}{\rho_l}}. \tag{15}$$

In detail, the characteristic time of bubble growth is proportional to δ. For example, for high-density ratios ($\delta \sim 10^{-3}$), then $t_c \sim 10^{-2}$ s, while $t_c \sim 10^{-9}$ s if the density ratio is low ($\delta \sim 10^{-1}$). In this problem $\rho_g \sim 10^2$ kg/m^3, while $\rho_l \sim 10^3$ kg/m^3, that is, $\delta \sim 10^{-1}$, so it is reasonable to consider that equilibrium is reached instantly.

After equilibrium is reached, there is a two-phase mixture in the lower control volume $\mathcal{V}_m$, as well as Halon 1301 and nitrogen both in vapor phase

in the upper control volume $\mathcal{V}_b - \mathcal{V}_m$. At $t = t_1$, the values of the saturated properties are obtained (see Appendix B.2): bottle pressure p_{b_1}, mixture volume V_m, mixture density ρ_{m_1}, liquid and vapor densities, ρ_{l_1} and ρ_{g_1}, void fraction α_{m_1} and compositions $\mathcal{X}_{k_1}$ and $\mathcal{Y}_{k_1}$. Moreover, due to the expected thermal non-equilibrium between the liquid and gas phases at the end of Step 1, a single mass-averaged temperature is considered for the whole bottle:

$$T_1 = \frac{m_{l_1} T_{l_1} + m_{g_1} T_{g_1}}{m_{l_1} + m_{g_1}}, \tag{16}$$

where m_{l_1} and m_{l_1} are bottle liquid and gas masses at the end of Step 1. As void fraction equals 1 in the upper control volume $\mathcal{V}_b - \mathcal{V}_m$, bottle mean void fraction α_{b_1} and density ρ_{b_1} are obtained as follows:

$$\alpha_{b_1} = 1 - \frac{V_m}{V_b}(1 - \alpha_{m_1}); \quad \rho_{b_1} = \alpha_{b_1}\rho_{g_1} + (1 - \alpha_{b_1})\rho_{l_1}. \tag{17}$$

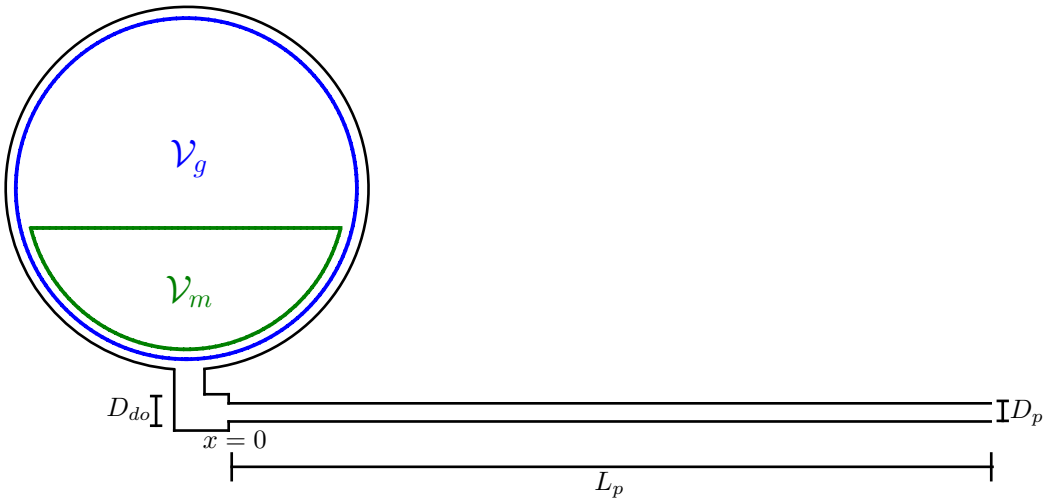

Figure 4: Control volumes corresponding to the system of equations of Step 2

Once the initial conditions of Step 2 are defined, in what follows it will be assumed that all the liquid stays in the steady control volume $\mathcal{V}_m$. Moreover, the thermodynamic properties of the vapor created in $\mathcal{V}_m$ and the ones of the vapor of $\mathcal{V}_b - \mathcal{V}_m$ are assumed to be the same at all times.

Another important aspect to consider is if the bubbles present in the control volume $\mathcal{V}_m$ will move upward to the control volume $\mathcal{V}_b - \mathcal{V}_m$ because

of buoyancy forces. During the initial stages of Step 2, $\alpha_m \ll 1$ and bubble diameters are small, so buoyancy forces will be negligible. Indeed, assuming $Re_{bub} \ll 1$ and considering Stokes' law for the drag, then terminal velocity $v_{ter} \sim \rho_l r_{bub}^2 g/\mu_l$. Bottle characteristic velocity $v_{c_b} \sim l_{c_b}/t_{c_d}$, and setting characteristic bottle length $l_{c_b} \sim 10^{-1}$ m and discharge time $t_{c_d} \sim 1$ s, then $v_{ter}/v_{c_b} \sim 10^{-3} \ll 1$ for $\rho_l \sim 10^3$ kg/m^3, $r_{bub} \sim 10^{-6}$ m, $g \sim 10$ m/s^2 and $\mu_l \sim 10^{-4}$ Pa $\cdot$ s. In latter stages, the committed error is assumed to be in the order of the one related to the condition of Step 2 finish (32).

Taking into account the previous remarks, continuity and energy equations applied to the control volume $\mathcal{V}_b$, together with species continuity and chemical equilibrium equations are:

$$\begin{cases} \dfrac{\mathrm{d}\rho_b}{\mathrm{d}t} = -\dfrac{v_{p_0} A_p}{V_b}\rho_m \quad \text{in } \mathcal{V}_b \times [t_1, t_2]; & (18) \\ \dfrac{\mathrm{d}e_b}{\mathrm{d}t} = -\dfrac{v_{p_0} A_p p_b}{\rho_m V_b} \quad \text{in } \mathcal{V}_b \times [t_1, t_2]; & (19) \\ \dfrac{\mathrm{d}\mathcal{Z}_k}{\mathrm{d}t} = 0 \quad \text{in } \mathcal{V}_b \times [t_1, t_2]; & (20) \\ \hat{f}_k^l = \hat{f}_k^g \quad \text{in } \mathcal{V}_b \times [t_1, t_2]; & (21) \\ \rho_b = \rho_{b_1},\ T_b = T_1,\ p_b = p_{b_1},\ \mathcal{Z}_k = \mathcal{Z}_{k_1} \quad \text{on } \mathcal{V}_b \times \{t_1\}. & (22) \end{cases}$$

For the bottle multiphase mixture, mean composition is defined as $\mathcal{Z}_k = \alpha_b \mathcal{Y}_k + (1 - \alpha_b)\mathcal{X}_k$. In addition, it has to be noted that the variable of the equation (19) is internal energy e, while the initial condition (22) is expressed in terms of temperature. In order to link both variables we have [4]:

$$\rho_b e_b = \alpha_b \rho_g (e_o + L_v + c_v(T_b - T_0)) + (1 - \alpha_b)\rho_l (e_o + c_l(T_b - T_0)), \quad (23)$$

being L_v latent heat of vaporization (see (C.6)) and $e_o = c_l T_0$ internal energy at a reference state. In regards to the density of the fluid in the control volume $\mathcal{V}_m$ appearing in the equations (18) - (19), ρ_m, the value is obtained from (17), together with the definition of mixture density:

$$\rho_m = \alpha_m \rho_g(T_b, \mathcal{X}_k) + (1 - \alpha_m)\rho_l(T_b, \mathcal{X}_k), \quad (24)$$

where the values of ρ_g and ρ_l are the same for ρ_m and ρ_b. In order to minimize the computational cost, during Step 2 saturated properties are precomputed for a suitable range of temperatures and compositions, and an interpolation of 4th order is performed in order to recover the values.

The differential equations along the pipe are presented (25) - (31), where λ is given by (14) with $Re = Re_{p_0}$. As equation (31) shows, bottle outlet pressure equals ambient pressure if possible; that is, if Mach number $M < 1$. If this is not the situation, then pipe outlet boundary condition will be $M = 1$ and the mass flow rate will be the critical, that is, the maximum value of G such that the slope of the pressure curve is negative. Furthermore, the value of internal energy at pipe inlet $\hat{e}_m$ is the one such that (30) is satisfied.

$$
\begin{cases}
v\dfrac{\partial \rho}{\partial x} + \rho\dfrac{\partial v}{\partial x} = 0 \quad \text{in } [0, L_p] \times [t_1, t_2]; & (25)\\
\rho v\dfrac{\partial v}{\partial x} = -\dfrac{\partial p}{\partial x} - \rho\lambda\dfrac{v^2}{2D_p} \quad \text{in } [0, L_p] \times [t_1, t_2]; & (26)\\
\rho v\dfrac{\partial e}{\partial x} = -p\dfrac{\partial v}{\partial x} + \rho\lambda\dfrac{v^3}{2D_p} \quad \text{in } [0, L_p] \times [t_1, t_2]; & (27)\\
\dfrac{\partial \mathcal{X}_k}{\partial x} = \dfrac{\partial \mathcal{Y}_k}{\partial x} = 0 \quad \text{in } [0, L_p] \times [t_1, t_2]; & (28)\\
\hat{f}_k^l = \hat{f}_k^g \quad \text{in } [0, L_p] \times [t_1, t_2]; & (29)\\
\rho = \rho_m,\ e = \hat{e}_m,\ \mathcal{X}_k = \mathcal{X}_{k_b},\ \mathcal{Y}_k = \mathcal{Y}_{k_b} \text{ and} \\
p = p_b - \dfrac{1}{2}\rho_m v_{p_0}^2\Big(\dfrac{A_p}{A_{do}}\Big)^2\left\{\Big(\dfrac{A_{do}}{A_p}\Big)^2 + \lambda\dfrac{L_{do}}{D_{do}}\right\} \quad \text{on } \{0\} \times [t_1, t_2]; & (30)\\
v = \dfrac{G_c}{\rho_m A_p} \quad \text{on } \{0\} \times [t_1, t_2] \ \Big|\Big|\ p = p_a \quad \text{on } \{L_p\} \times [t_1, t_2]. & (31)
\end{cases}
$$

With the objective of setting the condition for the end of Step 2, it is considered that the lower control volume $\mathcal{V}_m$ consists of a sum of cubes of side d, each one containing a bubble of radius $r = r(t)$ (see Figure 5). When $r = d/2$, then all the bubbles are in contact, and the void fraction of the lower control volume $\mathcal{V}_m$ is the ratio between the volume of a sphere of radius r and a cube of side d, that is:

$$\alpha_m = \frac{\pi}{6}. \tag{32}$$

When this condition is met, we consider that Step 3 starts.

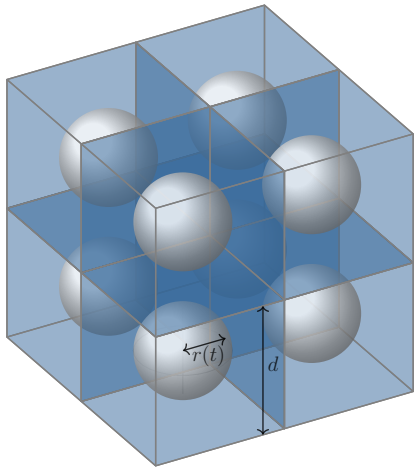

Figure 5: Bubble arrangement in control volume $\mathcal{V}_m$

2.2.3. Step 3

The last step consists of the discharge of Halon 1301 and nitrogen in gaseous phase, and finishes ($t = t_3$) when bottle pressure equals ambient pressure.

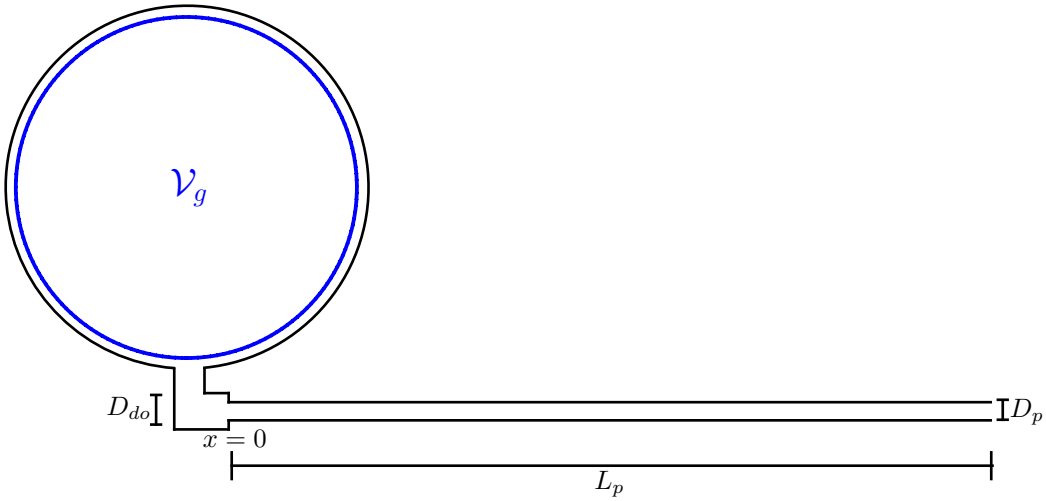

Figure 6: Control volume corresponding to the system of equations of Step 3

Assuming that the gas is calorically perfect, continuity and energy equations applied to the control volume $\mathcal{V}_g$, in addition to the equation of state are shown hereafter (33) - (37).

$$
\begin{cases}
\dfrac{\mathrm{d}\rho_g}{\mathrm{d}t} = -\dfrac{v_{p_0} A_p}{V_b}\rho_g \quad \text{in } \mathcal{V}_g \times [t_2, t_3]; & (33)\\
\dfrac{\mathrm{d}T_g}{\mathrm{d}t} = -\dfrac{v_{p_0} A_p p_b}{c_v \rho_g V_b} \quad \text{in } \mathcal{V}_g \times [t_2, t_3]; & (34)\\
\rho_g = \dfrac{p_b W_g}{\hat{Z}^v R T_g} \quad \text{in } \mathcal{V}_g \times [t_2, t_3]; & (35)\\
\rho_g = \rho_{g_1} \mid\mid \rho_{g_2},\ T_g = T_{g_1} \mid\mid T_2, & (36)\\
p_b = p_{b_1} \mid\mid p_{b_2},\quad \mathcal{Y}_k = \mathcal{Y}_{k_0} \mid\mid \mathcal{Y}_{k_3} \quad \text{on } \mathcal{V}_g \times \{t_2\}. & (37)
\end{cases}
$$

As (37) shows, initial conditions depend on whether Step 2 is present or not. In all cases the values of bottle variables are set equal to the ones at the end of the previous step, even though there is an important aspect to be taken into account in regards to the gas composition (37). If Step 2 is not present, then gas composition is equal to the one of the gas phase of Step 1. If it is present, then an equivalent composition $\mathcal{Y}_{k_3}$ is computed by following the reasoning explained in Section 2.2.4.

On the subject of pipe equations, introducing enthalpy, h, the theory of isentropic nozzle flow is taken as starting point [23]. Then, the effect of wall friction is added, where λ is given by (14) with $Re = Re_{p_0}$, and leads to the system of algebraic equations (38) - (44).

$$
\begin{cases}
v\dfrac{\partial \rho}{\partial x} + \rho\dfrac{\partial v}{\partial x} = 0 \quad \text{in } [0, L_p] \times [t_2, t_3]; & (38)\\
\rho v\dfrac{\partial v}{\partial x} = -\dfrac{\partial p}{\partial x} - \rho\lambda\dfrac{v^2}{2D_p} \quad \text{in } [0, L_p] \times [t_2, t_3]; & (39)\\
\dfrac{\partial}{\partial x}\Big(h + \dfrac{v^2}{2}\Big) = 0 \quad \text{in } [0, L_p] \times [t_2, t_3]; & (40)\\
\rho = \dfrac{pW_g}{RT} \quad \text{in } [0, L_p] \times [t_2, t_3]; & (41)\\
h = \dfrac{\gamma}{\gamma - 1}\dfrac{p_b}{\rho_g}, & (42)\\
p = p_b - \dfrac{1}{2}\rho_g v_{p_0}^2 \Big(\dfrac{A_p}{A_{do}}\Big)^2 \Bigg\{ \Big(\dfrac{A_{do}}{A_p}\Big)^2 + \lambda\dfrac{L_{do}}{D_{do}} \Bigg\} \quad \text{on } \{0\} \times [t_2, t_3]; & (43)\\
v = \dfrac{G_c}{\rho_g A_p} \quad \text{on } \{0\} \times [t_2, t_3] \;\Big|\Big|\; p = p_a \quad \text{on } \{L_p\} \times [t_2, t_3]. & (44)
\end{cases}
$$

It is important to remark that ideal gas equation of state is used (41), as the speed of sound has an analytical solution that reduces the computational cost, $a_{g_{id}} = \sqrt{\gamma p/\rho}$, being γ the specific heat ratio. In addition, pipe characteristic pressure $p_{c_3} \sim p_o$, so compressibility factor $\hat{Z}^v \approx 1$.

2.2.4. Transitions between steps

Sections 2.2.1, 2.2.2 and 2.2.3 have shown the proposed model for Steps 1, 2 and 3. However, some additional conditions are required in order to couple the results given by each system of equations.

Bottle equations

As previously explained, starting from the initial conditions (ICs), Figure 7 summarises the conditions that have to be satisfied in order to switch from one step into another.

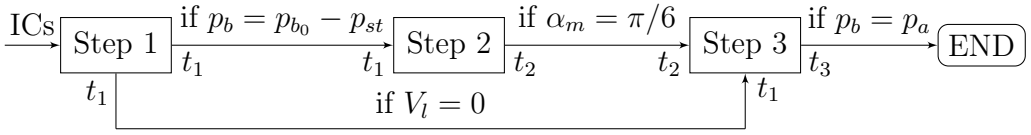

Figure 7: Diagram of step finishing conditions in terms of bottle equations

Pipe equations

With respect to pipe equations, the model proposed in Section 2.2 is valid only if the pipe is full of a single fluid, that is, the liquid from Step 1, the two-phase mixture from Step 2 or the gas from Step 3. This is not the situation during the transitions between steps, so a different approach has to be followed in these cases. Consequently, the goal of this section is to explain how the previous system of equations is adapted during pipe filling and the transitions between Steps 1 and 2, Steps 1 and 3 and Steps 2 and 3.

Pipe filling. Liquid mass flow rate takes its maximum value after the valve is opened, and it is calculated setting $L_p \to 0$. This gives a value for the velocity, that allows to obtain the position of the liquid front, x_f, for the next iteration. The process is repeated until $x_f = L_p$ at $t_{fill} \in [0, t_1]$. If the bottle runs out of liquid or bottle pressure equals bubble growth pressure, then all the previous calculations are neglected and the discharge starts again, now without taking into account the effect of surface tension; that is, there is no Step 1, so the new initial conditions are given by Appendix B.2.

Steps 1 and 2. At the end of Step 1, the pipe will be full of liquid. From this moment, it is assumed that the pressure profile at the end of Step 1, $p = p(x, t_1)$, as well as liquid velocity, $v = v(t_1)$, do not vary until the pipe runs out of liquid. In addition, density and temperature of the two-phase mixture are considered to be equal to bottle density and temperature. Following the same reasoning as in pipe filling, it is possible to calculate the position of the interface between the liquid and the two-phase mixture, x_{int}, at each instant until the transition is finished at $t_{12} \in [t_1, t_2]$.

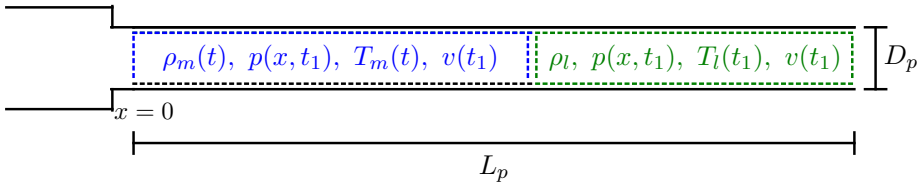

Figure 8: Values of the variables during transition between Steps 1 and 2

Steps 1 and 3. The reasoning is the same as the one corresponding to the previous paragraph, leading to the situation shown in Figure 9 until the gas-liquid interface reaches pipe outlet at $t_{13} \in [t_1, t_3]$.

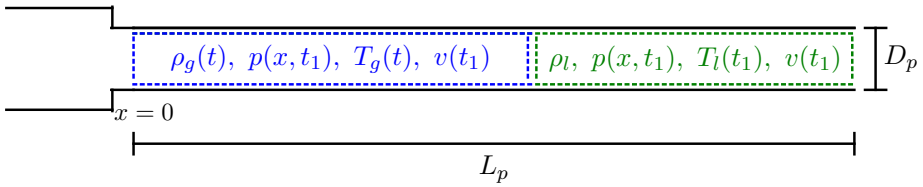

Figure 9: Values of the variables during transition between Steps 1 and 3

Steps 2 and 3. In regards to pipe flow, the approach explained in the previous paragraphs applies until $t_{23} \in [t_2, t_3]$. However, after Step 2 is finished, an issue arises regarding gas composition, as $\alpha_b(t_2) \neq 1$ because of the constraint (32). If the fluid is considered to be a heavy gas, a first approach may consist of assuming that the gas composition at the end of Step 2 is conserved. Nevertheless, bottle pressure at the end of Step 2 will not be the same as the pressure obtained by the equation of state from Step 3, so a discontinuity will arise in bottle pressure. This approach is not realistic, as shown by previous experiments [15, 32].

An alternative to ensure the continuity of the bottle pressure is to perform an iterative process. The goal is to obtain the gas equivalent composition, $\mathcal{Y}_{k_3}$, which is the composition that gives, by means of the equation of state, a value of bottle pressure equal to the saturation pressure at the end of Step 2. However, as in the case of bubble growth at the beginning of Step 2, gas composition will suffer a discontinuity. The real composition is expected to be a smoother profile than the one of the present model.

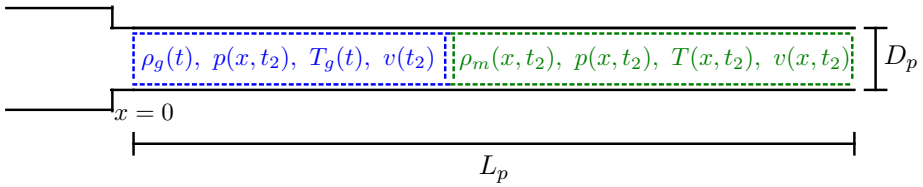

Figure 10: Values of the variables during transition between Steps 2 and 3

2.3. Numerical implementation

During Step 1 mass flow rate (11) is calculated making use of MATLAB function *fminbnd*, which is based on golden section search and parabolic interpolation [18]. Moreover, bottle equations (1) - (7) are solved by means of a 4th order Runge-Kutta scheme (*RK4*) [6], as well as MATLAB function *fsolve* to obtain bottle pressure (6). It makes use of the trust region *dogleg* algorithm, which is a variant of an older method [29]. After computing the mass flow rate, pressure distribution is obtained directly (9), and *fsolve* is employed to obtain the temperature distribution (10).

Secondly, during Step 2 the pipe is divided into n equispaced nodes, and finite differences [20] are employed for the spatial discretization of the system of equations (25) - (31). At pipe outlet backward finite differences are proposed, while centered finite differences are used in the rest of the nodes. Once the system of equations is spatially discretized, *fsolve* is employed to solve it with the aid of the proposed numerical method for the chemical equilibrium (see Appendix B.3). Then, *fminbnd* is used for the minimization problems associated to mass flow rate calculations, and *RK4* for the system of ordinary differential equations (18) - (22).

Finally, *fsolve* is used to solve the system of algebraic equations (38) - (44), while the numerical scheme *RK4* solves the system of ordinary differential equations (33) - (37) and *fsolve* gives the value of bottle pressure (35).

Step	Mass flow	Bottle equations	Pipe equations
1	*fminbnd*	*RK4*, *fsolve*	Analytical solution
2	*fminbnd*	*RK4*, *fsolve*	Finite differences, *fsolve*
3	*fsolve*	*RK4*	*fsolve*

Table 1: Methods used to compute the mass flow rate, as well as to solve the systems of equations

2.4. Limitations of the model

Numerous assumptions have been made in order to obtain the systems of equations, so it is important to keep in mind the principal weaknesses of the developed mathematical model. This will help to discuss the numerical results as effectively as possible, as well as to set new goals in terms of model improvements.

The proposed model assumes that the motion in the pipe is stationary, as a consequence of the high ratio between bottle and pipe residence times. However, during the transitions between steps, there is an interface between two different fluids that travels along the pipe. This leads to an unsteady process, so the approach followed in Section 2.2.4 is not probably able to capture the flow characteristics in this case. The fact of considering that pipe outlet mass flow rate is constant and the velocity of the two fluids is the same are restrictive assumptions, and the associated error is expected to increase with pipe length. This is because velocity decreases proportionally with pipe length, due to the friction term appearing in the momentum equation, so transitions last longer.

A one dimensional approach has been followed in terms of the geometry. Together with the incompressibility assumption, an important result is that liquid evaporates at pipe outlet during Step 1. Nevertheless, the flow is expected to be turbulent, as $Re = \rho v D_p/\mu \sim 10^6 \gg Re_t$ for $\rho \sim 10^3$ kg/m^3, $v \sim 10$ m/s, $D_p \sim 10^{-2}$ m and $\mu \sim 10^{-4}$ Pa $\cdot$ s. This results in the existence of three dimensional perturbations that can produce bubble growth, an effect that is further accentuated by the possible complex geometry of the discharge outlet. In addition, even if the mean flow variables serve as a good approximation of the problem, the applicability Darcy's law together with Colebrook-White to multiphase flows is unclear. This facts also underline additional errors caused by the steady assumption.

Another important aspect to take into account is that the pressure loss through the discharge outlet is proportional to pipe inlet velocity (see relationships (11), (30) and (43)). Focusing on Step 2, as density and fluid compositions are conserved (see (30)), the equilibrium condition produces that pressure loss is translated only into temperature variations. For large values of the mass flow rate, if mass diffusion is dominant during the transitions between different equilibrium states, then temperature may decrease notably and lead to incoherent pipe inlet temperature values.

To conclude, despite the weaknesses cited in the previous paragraphs, it has to be stressed that the first results given by the model are positive (see Section 3.1).

3. Results

In this section the results obtained by solving numerically the systems of equations (1) - (7), (8) - (12), (18) - (22), (25) - (31), (33) - (37) and (38) - (44) are discussed. For that purpose, first of all the accuracy of this model called *firex_upm* is tested taking as reference the results provided by a computer program developed by NASA, *HFlow* [15], as well as experimental results (Section 3.1). Then, another test case is simulated in order to observe the most important features of the problem (Section 3.2), and a parametric study is presented (Section 3.3).

3.1. Comparison with HFlow

HFlow is a tool programmed in Fortran in the early 80s, even though there have been subsequent updates. The values of some variables given by *HFlow* have been validated under specific conditions [15], so the first goal of the results section will be to test the accuracy of the model detailed before. Test 146 will be taken as reference [15].

As Figure 11 shows, the system used in Test 146 consisted of a bottle and a discharge outlet followed by a convergent nozzle. In order to measure bottle temperatures, two probes were placed at the top and at the bottom of the bottle. Moreover, the bottle was equipped with a pressure transducer.

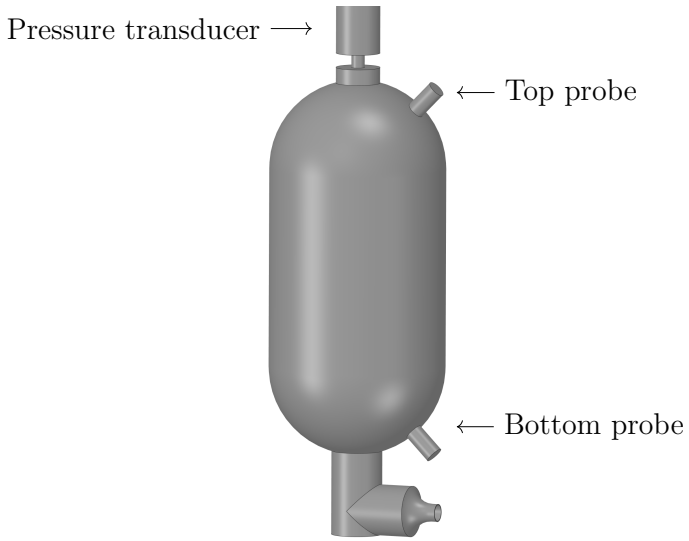

Figure 11: System corresponding to Test 146. Adapted from [15]

Due to lack of information in the previously cited article, it is not possible to match all the conditions of the experiments exactly. However, the experimental results obtained in Test 146 and numerical results given by *HFlow* will serve as a point of reference.

Table 2 provides the values of the parameters used in the simulations (see Appendix C). The work done by Snegirev and Lipjainen [30] has been taken as reference for thermodynamic properties, while [15] provides the values of the parameters related to geometry and initial conditions. It has to be noted that nozzle exit diameter has been taken as pipe diameter.

Symbol	**Parameter**	**Value**	**Units**
c_l	Liquid specific heat	862.56	$\mathrm{J/(kg \cdot K)}$
c_v	Gas specific heat at constant volume	470.817	$\mathrm{J/(kg \cdot K)}$
D_{do}	Discharge outlet diameter	$25.23 \cdot 10^{-3}$	m
D_p	Pipe diameter	$9.96 \cdot 10^{-3}$	m
$\mathrm{d}t$	Time step	0.001	s
L_{do}	Discharge outlet length	$75.6 \cdot 10^{-3}$	m
L_p	Pipe length	10^{-4}	m

L_v	Latent heat of vaporization	$8.216 \cdot 10^4$	J/kg
m_{h_0}	Halon 1301 mass	2.33	kg
n	Number of pipe nodes	10	–
p_a	Ambient pressure	101325	Pa
p_{b_0}	Initial bottle pressure	$5.17 \cdot 10^6$	Pa
T_0	Initial bottle temperature	294.15	K
V_b	Bottle volume	$2.76 \cdot 10^{-3}$	m^3
ε	Pipe rugosity	0	m
γ	Ratio of specific heats	1.216	–
σ	Halon 1301 surface tension	$4.5 \cdot 10^{-3}$	N/m

Table 2: Parameters used to simulate Test 146

Focusing attention on the comparison of the numerical and experimental results, firstly, the temperature measured by the bottom probe is given by Figure 12a. It measures liquid temperature until the bottle runs out of liquid at $t \approx 0.8$ s, while the rest of the temperature values are related to the gas of Step 3. The graph shows that *HFlow* predicts lower liquid temperatures than the measured ones, in particular at the end of the discharge, when the differences increase up to 50 K. In contrast, the values given by our model *firex_upm* are more precise, and a maximum error of 10 K is maintained.

Secondly, Figure 12b provides the temperature measured by the top probe, that is, the temperature of the gas phase. With the exception of initial time steps, our curve matches almost perfectly at all times. As in the case of Figure 12a, *HFlow* is not accurate after the bottle runs out of liquid, and shows gas temperature values that differ notably from the experimental results.

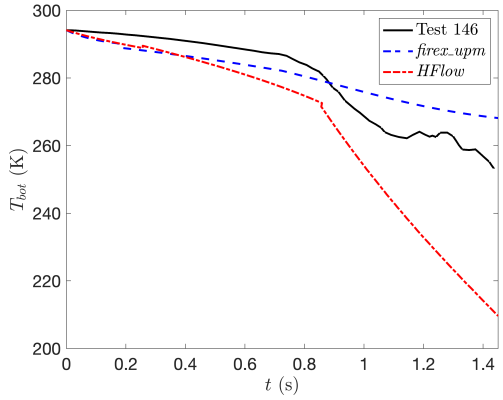

(a) Bottom probe temperature

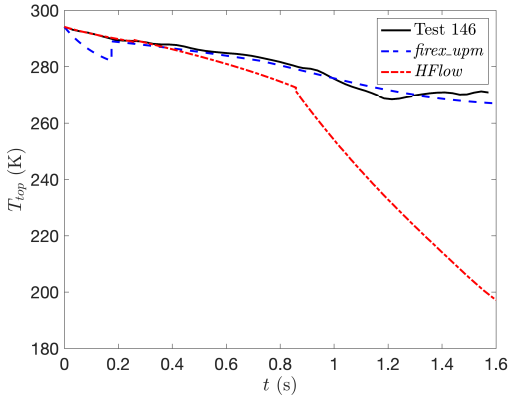

(b) Top probe temperature

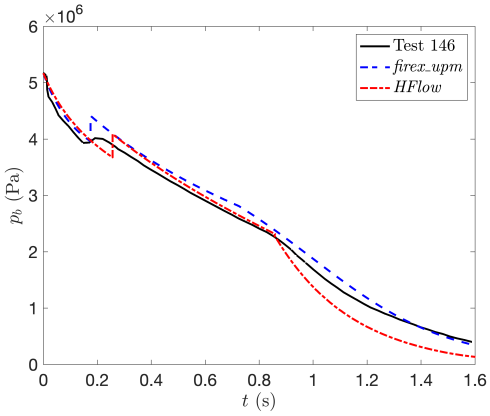

(c) Pressure

Figure 12: Bottle thermodynamic variables from Test 146 [15], the method developed in this paper and *HFlow* [15]

Finally, Figure 12c shows that the three curves are similar until $t \approx 0.2$ s, that is, when bottle pressure equals saturation pressure minus the pressure exerted by surface tension. Even though bubble growth does not happen at the same time in both models, bottle pressure curves are similar, and numerical errors are of the same order of magnitude in both programs.

As a consequence of the above, it can be inferred that the developed model *firex_upm* is highly accurate, as the results given by the program are in great

agreement with the experimental data. It is important to highlight that, in contrast to *HFlow*, the model does not depend on parameters that have been adjusted for these specific conditions. The model *firex_upm* is highly reliable, as a consequence of the solid thermodynamic basis. This is demonstrated in Appendix A, where some thermodynamic approximations used in the literature are compared with the approach followed in this work (Appendix B.3). Moreover, the effects of those approximations in the accuracy of the model can be observed.

3.2. Case of practical application

Once it has been done a first study of the accuracy of the model, in this section the results corresponding to a different configuration will be presented. The system is assumed to consist of a spherical bottle, a discharge outlet and a pipe (see Figure 1). Table 3 shows the values of the parameters, which are representative of a case of civil aviation in flight conditions.

Symbol	**Parameter**	**Value**	**Units**
c_l	Liquid specific heat	800.684	$\mathrm{J/(kg \cdot K)}$
c_v	Gas specific heat at constant volume	561.749	$\mathrm{J/(kg \cdot K)}$
D_{do}	Discharge outlet diameter	0.03	m
D_p	Pipe diameter	0.03	m
$\mathrm{d}t$	Time step	0.001	s
L_{do}	Discharge outlet length	0.15	m
L_p	Pipe length	1	m
L_v	Latent heat of vaporization	$1.049 \cdot 10^5$	J/kg
m_{h_0}	Halon 1301 mass	8	kg
m_{n_0}	Nitrogen mass	0.5	kg
n	Number of pipe nodes	10	–
p_a	Ambient pressure	101325	Pa
T_0	Initial bottle temperature	248.15	K
V_b	Bottle volume	0.01	$\mathrm{m^3}$
ε	Pipe rugosity	$1.5 \cdot 10^{-6}$	m

γ	Ratio of specific heats	1.321	–
σ	Halon 1301 surface tension	0.011	N/m

Table 3: Parameters used for the simulation of the case of practical application

After setting the values of the parameters, first of all, Figure 13a shows that the variations in liquid temperature are negligible with respect to the gas case; indeed, liquid temperature decreases a few K until the bottle runs out of liquid at $t \approx 0.15$ s. From this point in time, there is only gas in the bottle, and bottle temperature decreases rapidly until reaching a value of $T_g \approx 150$ K at $t \approx 0.35$ s.

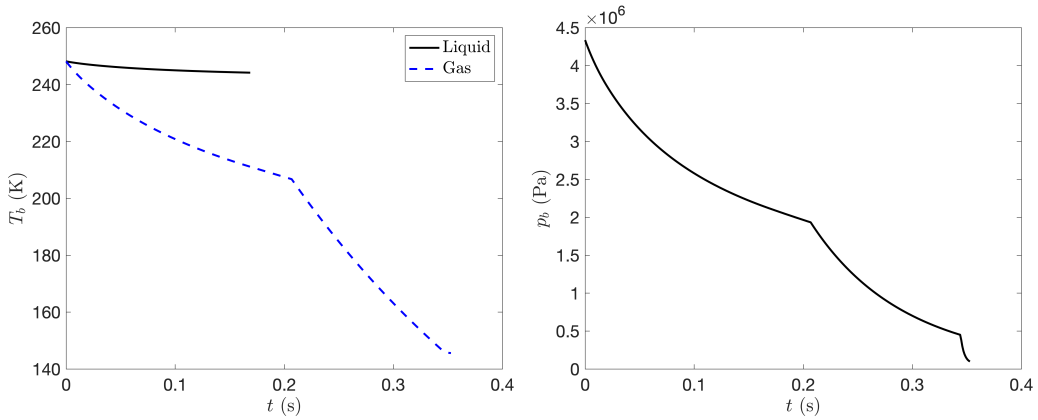

(a) Liquid and gas temperatures

(b) Pressure

Figure 13: Bottle thermodynamic variables given by the method developed in this paper, *firex_upm*, for a case of practical application

Secondly, bottle pressure as a function of time can be seen plotted in Figure 13b, where the first approximately linear drop is followed by a slower decrease until $t \approx 0.2$ s. It is worth noting that bottle pressure is $p_b \approx 2$ MPa at this instant of time; this value is greater than bubble growth pressure (see equation (13)), so in this case there is no two-phase flow. Finally, bottle pressure decays rapidly until reaching ambient pressure at $t \approx 0.35$ s, in a similar way as in the gas temperature case.

From the moment when the last liquid leaves the bottle, the proposed model assumes that liquid and gas velocities do not vary until the pipe is full

of gas. This is the reason why the first drop in the pipe outlet mass flow rate is followed by an interval where it is constant (Figure 14a). When the exit fluid changes from liquid to gas, velocity increases but the density decrease is larger, and this causes the important mass flow rate decay at $t \approx 0.2$ s.

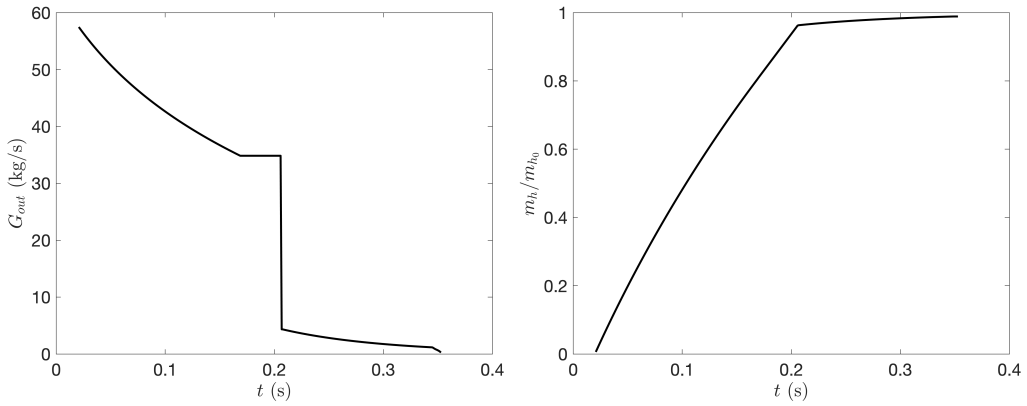

(a) Outlet mass flow rate (b) Halon mass expelled

Figure 14: Pipe variables given by the method developed in this paper, *firex_upm*, for a case of practical application

Finally, the curve related to the Halon mass expelled (divided by the initial Halon mass) shows that most of the Halon is expelled during Step 1. It must be emphasized that at $t \approx 0.2$ s more than 95% of the initial Halon mass has been expelled. When bottle pressure equals ambient pressure, only a marginal quantity of the initial Halon mass remains in the bottle (0.5%).

3.3. Parametric study

The results section will be finished with a study of the influence of some key parameters. This allows not only to acquire intuitive ideas about the flow behaviour, but also to know which changes may be required if the previous results are not sufficient to meet the requirements of a fire extinguishing system.

3.3.1. Halon mass

If the discharge is fast but there is not enough Halon in the air, a first solution may consist of an Halon mass increase in the bottle. Figures 15a - 15d show the differences if Halon mass is increased or decreased by 2 kg.

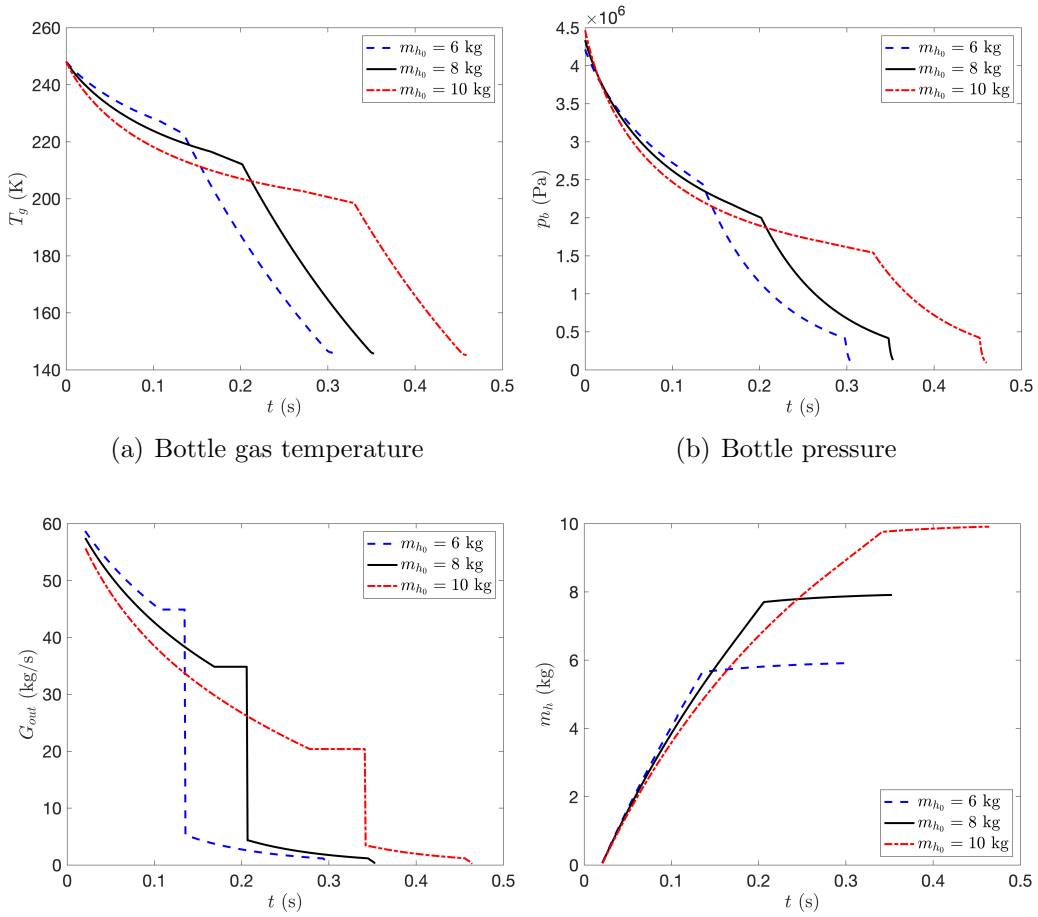

(a) Bottle gas temperature

(b) Bottle pressure

(c) Pipe outlet mass flow rate

(d) Halon mass expelled

Figure 15: Variables of the problem given by the method developed in this paper, *firex_upm*, for three different values of initial Halon mass

The fact of modifying Halon mass does not have a great impact on the results, as initial bottle pressure is not practically affected by the variations of this parameter (Figure 15b). If initial Halon mass decreases, so does the amount of liquid in the bottle, and Step 1 takes less time to finish as mass flow rate is larger (Figure 15c). This is because liquid composition is not the same in each case, causing differences in the thermodynamic curves, which are definitely relevant in this problem. In addition, in the 10 kg case, velocity is reduced at the end of the Step 1, that is, it takes more time to the liquid front to reach pipe outlet, so the time interval of constant mass flow rate

is bigger. Although at intermediate times ($t \approx 0.15$ s) the expelled mass is higher in the case of lower initial mass, in all cases more than 95% of the Halon initial mass is outside the system at $t \approx 0.35$ s (Figure 15d).

3.3.2. Nitrogen mass

Initial nitrogen mass can also be modified. Nitrogen pressurizes the Halon, so, if nitrogen mass is higher, then bottle pressure increases. However, the effects of this modification in other variables are not clear.

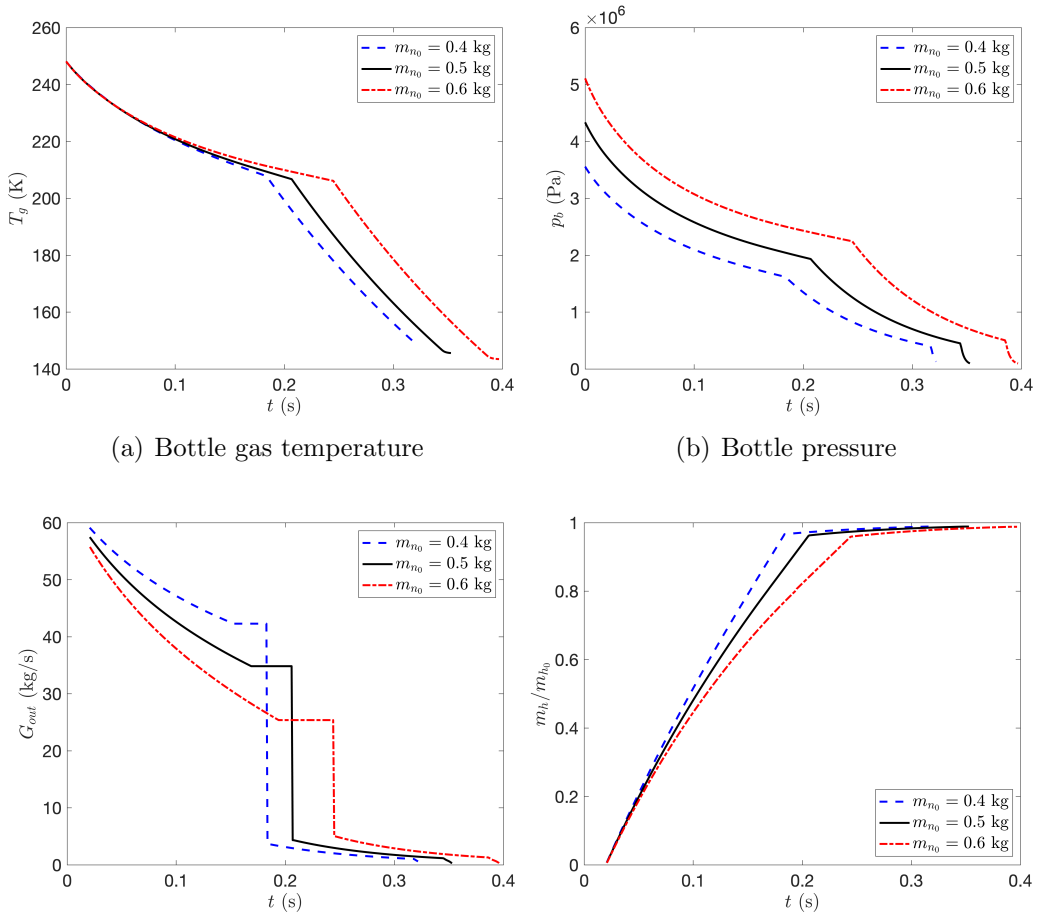

(a) Bottle gas temperature

(b) Bottle pressure

(c) Pipe outlet mass flow rate

(d) Halon mass expelled

Figure 16: Variables of the problem given by the method developed in this paper, *firex_upm*, for three different values of initial nitrogen mass

Figures 16a - 16d demonstrate that small modifications in nitrogen mass produce significant changes in mass flow rate and bottle pressure, the last one increasing proportionally with nitrogen mass. This result is consistent, as a bigger amount of nitrogen is dissolved in Halon, which raises the saturation pressure of the mixture. With respect to mass flow rate differences, the reasoning followed in the case of the influence of Halon mass also applies.

It must be stressed that whenever deciding bottle definitive configuration, if bottle pressure is lowered, then the mechanical resistance required for bottle and discharge outlet junctions is reduced. Bottle pressure and discharge time decrease as nitrogen mass decreases, so a question arises: is there any quantity that minimizes the discharge time, while keeping low values of bottle pressure?

The answer of the question is given by Figures 17a and 17b. In this situations discharge time does not increase inversely proportional to nitrogen mass, as there is an optimum value of nitrogen mass between 0.3 kg and 0.5 kg. The reason of this fact lies in the exit pressure, which is higher than ambient pressure for $m_{n_0} = 0.5$ kg, but it decreases, increasing the mass flow rate, until reaching it when $m_{n_0} \approx 0.4$ kg; from that optimum point, mass flow rate decreases proportionally to nitrogen mass; that is, the pipe admits a maximum value of mass flow rate.

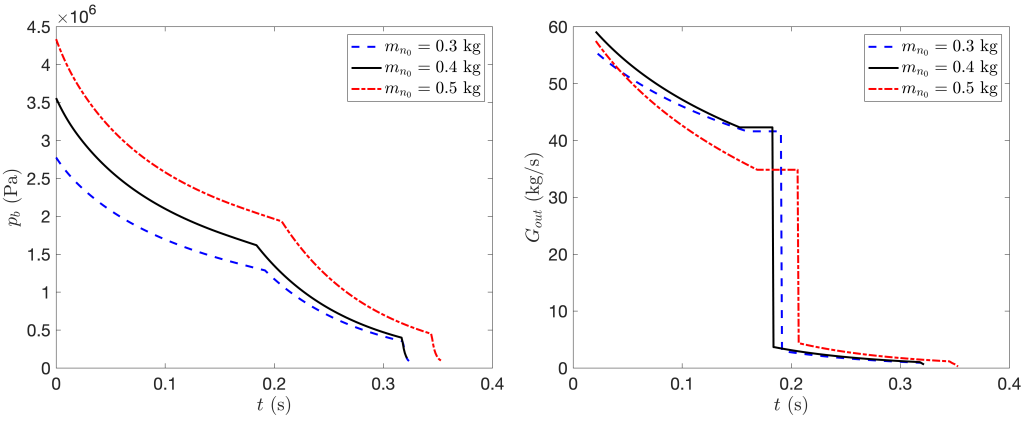

(a) Bottle pressure

(b) Pipe outlet mass flow rate

Figure 17: Variables of the problem given by the method developed in this paper, *firex_upm*, for three different values of initial nitrogen mass

3.3.3. Initial temperature

Initial temperature can vary depending on the application; for example, flight conditions can be modified, so it is interesting to analyse the effect of this parameter in the discharge process. As some of the parameters of the problem depend on initial temperature, Table 4 shows the values of the modified parameters.

Symbol	$\boldsymbol{T_0 = 218.15}$ **K**	$\boldsymbol{T_0 = 288.15}$ **K**	**Units**
c_l	769.697	853.507	$\mathrm{J/(kg \cdot K)}$
c_v	643.236	485.348	$\mathrm{J/(kg \cdot K)}$
L_v	$1.159 \cdot 10^5$	$8.579 \cdot 10^4$	J/kg
γ	1.369	1.237	–
σ	$1.52 \cdot 10^{-2}$	$5.3 \cdot 10^{-3}$	N/m

Table 4: Modified parameters for $T_0 = 218.15$ K and $T_0 = 288.15$ K

Figures 18a and 18b show that the discharge time is proportional to temperature. This is due to the fact that Halon surface tension decreases with temperature (C.10), so the pressure exerted by surface tension follows the same behaviour (13). Consequently, the pressure difference between bottle and pipe outlet is reduced, allowing a lower value of the mass flow rate.

Calling attention to the case of $T_0 = 288.15$ K, the low value of surface tension at that temperature leads to reach bubble growth pressure fast, and Step 2 starts at Point A ($t_1 \approx 0.1$ s). As pipe liquid velocity is lower than in the other two cases (Figure 18c), the transition between phases extends more (segment AB). After Point C there is a two-phase flow in the pipe, and mass flow rate decreases until Step 2 is finished at Point D ($t_2 \approx 0.3$ s). After the transition between Steps 2 and 3 is finished (Point E), despite the fact that the value of mass flow rate is higher than in the other cases, there is more Halon left in the bottle (Figure 18d), so Step 3 also lasts a longer period.

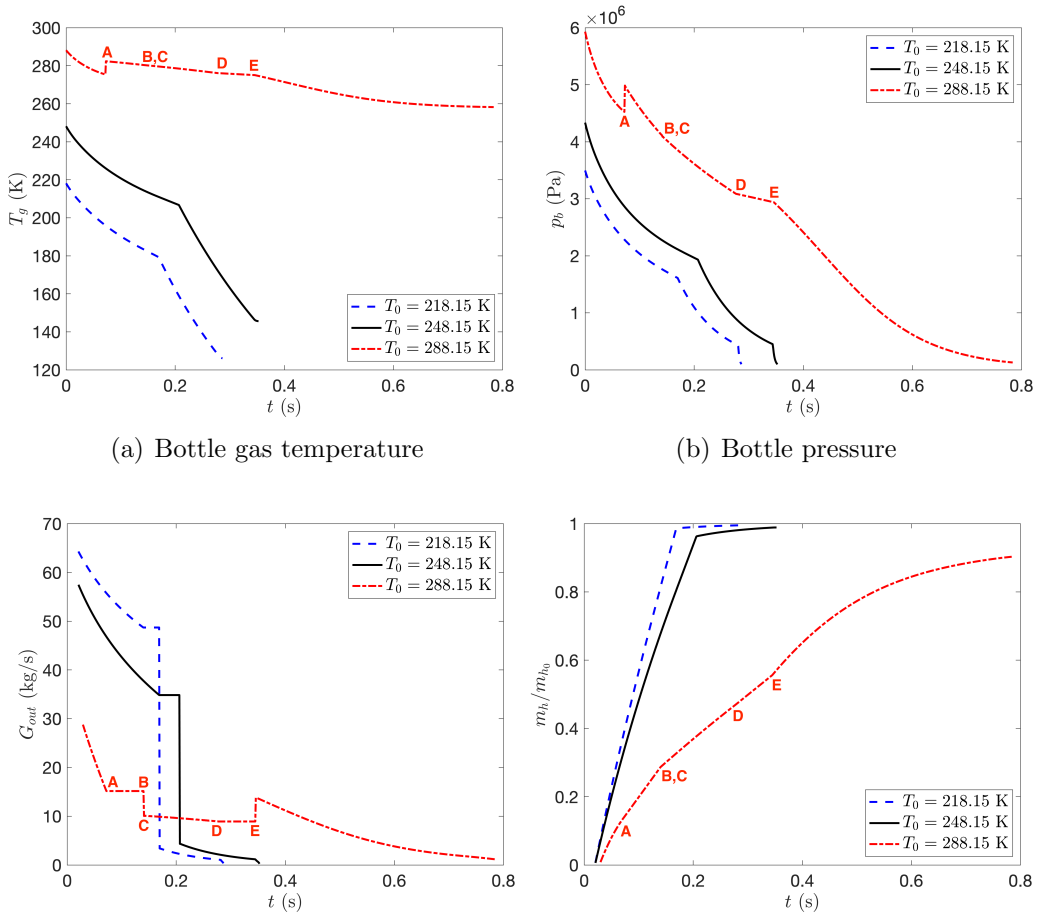

(a) Bottle gas temperature

(b) Bottle pressure

(c) Pipe outlet mass flow rate

(d) Halon mass expelled

Figure 18: Variables of the problem given by the method developed in this paper, *firex_upm*, for three different values of initial temperature

It is important to stress that, during the transition between Steps 2 and 3, the velocity of the two-phase mixture is used in the system of equations (33) - (37). As it is lower than the velocity of the gas from Step 3, this fact causes the sudden decrease in the slope of the pressure curve (Figure 18b, Point D). As mentioned in Section 2.4, the assumption of the constant velocity is one of the weak points of the model. Another remarkable difference is that the amount of Halon inside the bottle is important at the end of the discharge for the case of $T_0 = 288.15$ K. This is because the equivalent Halon gas mass fraction $\mathcal{Y}_{h_3}$ is close to 1 during Step 3.

4. Conclusions

In this work a mathematical model has been developed to study the discharge of a fire extinguishing agent. It has been divided into three parts, each one of them corresponding to a different discharge step. The initial equations have been simplified until obtaining a numerically solvable system, but that represents the most important features of the fluid motion. Experimental correlations in the thermodynamic part of the model have been avoided to widen the range of applicability of the model. The resulting system has been solved by means of finite difference formulas for the spatial discretisation, a Runge-Kutta scheme for the temporal discretisation and two MATLAB functions for the non-linear algebraic equations and minimization problems.

With respect to the results, on the one hand the comparison with *HFlow* and experimental results [15] has shown great accuracy of the developed model, *firex_upm*. Indeed, taking into account that the accurate values of all the parameters are not known, bottle variables are approximated notably. As bottle variables depend on pipe variables, the errors corresponding to other quantities as mass flow rate are not expected to be important. Despite the fact that the parameters of the model have not been adjusted from the experiment, the results are remarkably good.

On the other hand, a case of practical application has been simulated. An analysis of the influence of some parameters has been performed, starting with species mass; it has been shown that modifications in Halon mass do not alter the results, while nitrogen mass is a relevant parameter, as small changes produce important variations in bottle pressure. In addition, it has been noted the existence of an optimum value of nitrogen mass in terms of structural resistance, while keeping a low value of discharge time. The last study has been focused on the initial temperature, and has allowed to deduce that discharge time increases with initial temperature, caused by the decrease in Halon surface tension. The differences are further accentuated when there is a two-phase flow in the pipe.

Finally, it has to be stressed that the validity of the approach followed in some situations is unclear, for example in the case of the transitions between steps, as an unsteady process is modeled as steady. This case is not covered by the chosen experiment, as pipe length is very small. For this reason, it is necessary to conduct experiments with long pipes, as they may be helpful to detect additional weak points of the theory. For example, measurements of bottle pressure, bottle temperatures and pipe outlet mass flow rate would

provide useful information.

Acknowledgements

The authors acknowledge Airbus Operations and Universidad Politécnica de Madrid for their support and permission to publish this work. Additionally, Gonzalo Rubio acknowledges the funding received by the grant *Ayudas dirigidas al PDI para el fomento de la participación en solicitudes de proyectos H2020* from Universidad Politécnica de Madrid. Finally, the authors gratefully acknowledge the Universidad Politécnica de Madrid (www.upm.es) for providing computing resources on Magerit Supercomputer.

Appendix A. Thermodynamics

None of the previous studies found in the literature has used a real gas equation of state for the thermodynamic part of the models. Consequently, the aim of this appendix is to justify the need of such formulation to take into account the most relevant aspects of the discharge. The analysis will be focused on the saturation pressure and the speed of sound. An accurate calculation of these variables is important, as both impose limitations in the value of the mass flow rate. In addition, saturation pressure establishes the change from Step 1 to Step 2, and it is equal to the pressure of the two-phase mixture during Step 2.

Saturation pressure

For the calculation of the saturation pressure of the mixture during Step 2, three previous approaches used in the literature can be highlighted:

- Assume that no nitrogen dissolves in Halon, so the saturation pressure of the mixture is the one of Halon 1301 [21, 22].
- Consider that Henry's law is applicable, and compute all of the saturation properties by means of correlations (*HFlow*, [15]).
- Neglect the change of composition. Saturation pressure depends only on temperature [32].

First of all, Figure A.19a shows that the fact of assuming that nitrogen does not dissolve in Halon is not accurate, as the differences in saturation pressure are important. Moreover, the correlations used by NASA [15] give similar values as our model *firex_upm*. It has to be stressed that the calculation of the saturation pressure of Halon 1301 has been done by setting $\mathcal{X}_n = 10^{-3}$.

In principle, given the accuracy of *HFlow*, one may think that the use of real gas models is not justified. However, when there is only gas in the bottle, saturation pressure is no longer present in the calculations, and the equation of state is needed to obtain gas properties accurately. It has been shown in Figure 10 that gas temperature deviates notably in the case of *HFlow*, so additional correlations would be needed in this case. This can be a difficult task, as gas pressure is a function of temperature, density and composition.

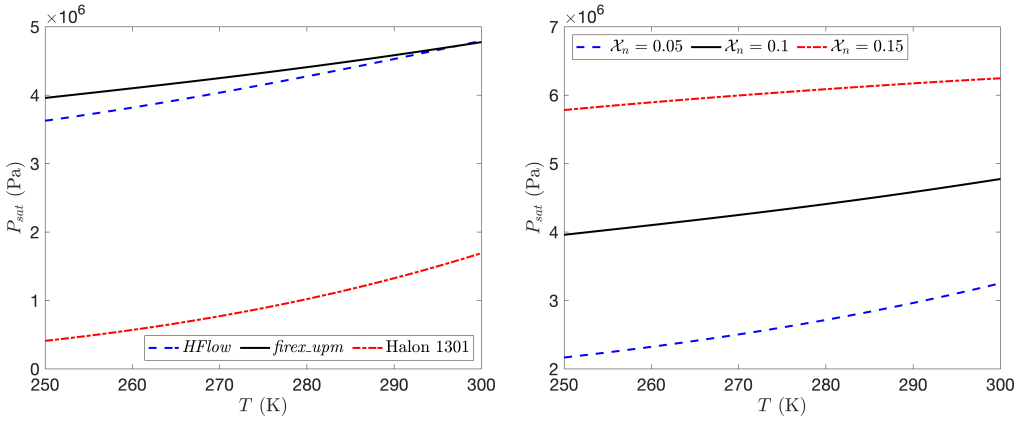

(a) Influence of the model

(b) Influence of liquid composition

Figure A.19: (a) Saturation pressure given by *HFlow* for $\mathcal{X}_n = 0.1$, our model *firex_upm* for $\mathcal{X}_n = 0.1$ and the one of Halon 1301. (b) Saturation pressure given by *firex_upm* for three different values of liquid composition

Finally, if saturation pressure depends only on temperature, Figure A.19b demonstrates that small changes in liquid composition produce significant modifications in saturation pressure. Moreover, in Test 146 the temperature of the two-phase mixture decreases less than 10K during Step 2 (see Figures 12a and 12b) while bottle pressure decreases around 2 MPa (see Figure 12c), so it is also shown that mass diffusion dominates against thermal diffusion

during bubble growth. Consequently, it can be concluded that the assumption of constant composition can induce important errors in the results.

Speed of sound

Except in the analysis of the influence of initial temperature, in none of the practical cases a two-phase discharge occurs. The argument based on the increase of surface tension allows to explain discharge time differences, as the presence of Step 2 produces a second-order effect. However, in the first result subsection (NASA's Test 146, [15]) it has been found that the two-phase discharge is slower than the liquid discharge. Surface tension is no longer important in this case, and it is necessary to further study the problem in order to understand how the two-phase flow consisting of Halon 1301 and nitrogen behaves.

When the discharge is carried out as a liquid, mass flow rate limitation is given by the saturation pressure, as the speed of sound is too high to be reached at pipe outlet. Friction losses are proportional to liquid density, a high value that causes low values of velocity to yield important pressure losses. For its part, gas densities are usually low, so it is easy to have $M = 1$ at pipe outlet. As previously mentioned (see Section 2.2.3), assuming ideal gas, the speed of sound is obtained directly, $a_{g_{id}} = \sqrt{\gamma p/\rho}$.

In two-phase mixtures, boundary conditions at pipe outlet are identical to the ones corresponding to the gas flow, although speed of sound is not obtained immediately. For this reason, it has to be calculated by means of an iterative method as the one explained in the theoretical content. Focusing attention in Test 146, the proposed approach yields values of mixture speed of sound $a_m \approx 20$ m/s, a much lower value than gas and liquid speed of sound, $a_g \approx 200$ m/s and $a_l \approx 250$ m/s (see [28] for more details of the calculation in this case).

In summary, an accurate calculation of the speed of sound is important in this problem. Only one of the previous studies has proposed a model to calculate it [32], based on the theory of characteristics [31]. However, no results are shown in terms of mass flow rate or fluid velocity, and some parameters are used to adjust the model. In contrast, the new method proposed in this work does not need any adjusting parameter. Moreover, it is based on the equation of state, whose results seem to be promising (see Section 3.1).

Appendix B. Chemical equilibrium

This appendix deals with the application of chemical equilibrium in two particular situations as the initial conditions (Appendix B.1) and the beginning of Step 2 (Appendix B.2). The numerical implementation in a general case is shown in Appendix B.3, and the range of validity of the code is explained in Appendix B.4.

Appendix B.1. Calculation of the initial conditions

Initially, the known variables are temperature T_0, bottle volume V_b, nitrogen mass m_{n_0} and Halon mass m_{h_0}. Assuming thermodynamic equilibrium, chemical equilibrium equation states [13]:

$$\hat{f}_k^l = \hat{f}_k^v, \tag{B.1}$$

where $\hat{f}_k^\epsilon$ is the fugacity of the specie k in the ϵ phase.

Given a liquid composition in mole fractions, $\mathcal{X}_k$, chemical equilibrium allows to compute saturation pressure, $p_{sat} = p_b$, liquid and gas compressibility factors, $\hat{Z}^l$ and $\hat{Z}^v$, and gas composition in mole fractions, $\mathcal{Y}_k$ (see Appendix B.3). Then, liquid and gas densities are directly calculated:

$$\rho_l = \frac{p_b W_l}{\hat{Z}^l R T_0}; \quad \rho_g = \frac{p_b W_g}{\hat{Z}^v R T_0}, \tag{B.2}$$

where W_l and W_g are liquid and gas molecular masses:

$$W_l = \sum_k \mathcal{X}_k W_k; \quad W_g = \sum_k \mathcal{Y}_k W_k. \tag{B.3}$$

At this point, liquid and gas densities and compositions are known, together with Halon and nitrogen masses. Therefore, it is possible to obtain liquid and gas masses, m_{l_0} and m_{g_0}, by solving a system of equations as follows:

$$\begin{bmatrix} X_1 & Y_1 \\ X_2 & Y_2 \end{bmatrix} \begin{bmatrix} m_{l_0} \\ m_{g_0} \end{bmatrix} = \begin{bmatrix} m_{n_0} \\ m_{h_0} \end{bmatrix}, \tag{B.4}$$

where X_k and Y_k are the mass fractions of the specie k corresponding to the liquid and gas phase, respectively:

$$X_k = \frac{\mathcal{X}_k W_k}{W_l}; \quad Y_k = \frac{\mathcal{Y}_k W_k}{W_g}. \tag{B.5}$$

Once m_l and m_g are calculated, liquid and gas volumes are obtained:

$$V_l = \frac{m_l}{\rho_l}; \quad V_g = \frac{m_g}{\rho_g}. \tag{B.6}$$

The volume condition states that $V_b = V_l + V_g$, so there will be a value of $\mathcal{X}_{k_0}$ that satisfies it, together with p_{b_0}, V_{l_0}, ρ_{l_0}, ρ_{g_0} and $\mathcal{Y}_{k_0}$. Therefore, an iterative process is done in order to obtain the solution. If there is more than one solution, the physically most coherent one is chosen.

Appendix B.2. Calculation of bottle conditions at the beginning of Step 2

As mentioned in Section 2.2.2, when bottle pressure equals bubble growth pressure, bubbles start to grow until equilibrium is reached. After this process, the bottle remains to be divided into two volumes (see Figure 4): the lower volume V_m with a two-phase mixture, and the upper volume $\mathcal{V}_b - \mathcal{V}_m$, where Halon 1301 + nitrogen is present in vapor phase. The goal of this section is to show the process that is carried out in order to have the bottle conditions well defined at $t = t_1$.

At the end of Step 1, some quantities are known: Halon 1301 mass in the liquid, m_{h_l}, nitrogen mass in the liquid, m_{n_l} and liquid volume, V_{l_1}. However, the value of the liquid volume is not useful, as bubble growth will produce liquid layer to raise; that is, $V_{m_1} > V_{l_1}$. The value of V_{m_1} is not known, neither equilibrium liquid composition, $\mathcal{X}_{k_1}$, so chemical equilibrium cannot be computed without making further assumptions.

As temperature T_1 is given by (16), considering that the lower and upper volumes are mixed, it is possible to obtain all the thermodynamic properties; in particular, bottle pressure p_{b_1}. Despite the fact that it is a virtual situation, the value p_{b_1} is set as bottle pressure at the beginning of Step 2, for both $\mathcal{V}_m$ and $\mathcal{V}_b - \mathcal{V}_m$. Therefore, there exist $\mathcal{X}_{k_1}$ and V_{m_1} such that the equilibrium computation in this upper volume gives a saturation pressure equal to p_{b_1}.

Appendix B.3. Numerical implementation

Chemical equilibrium equation (B.1) gives the saturation pressure of the mixture. In order to solve it, Peng-Robinson equation of state is used [27].

From the expressions of the fugacity coefficient for mixtures $\hat{\phi}_k$ (see [13, 27]), fugacity is computed by means of the relationship $\hat{\phi}_k = \hat{f}_k/(\mathcal{X}_k p)$, and an iterative process is performed until (B.1) is fulfilled. Accordingly, a MATLAB function has been done, whose features are explained in the next

paragraphs. It essentially computes the saturation pressure, together with vapor composition and compressibility factors.

First of all, it is necessary to obtain the molecular mass, critical properties and the acentric factor of both species, the objective being to compute Peng-Robinson equation single-component constants. Taking [3, 7] as references, Table B.5 shows the data in the case of Halon 1301 and nitrogen.

Component	**W (g/mol)**	$\boldsymbol{T_{cr}}$ **(K)**	$\boldsymbol{p_{cr}}$ **(MPa)**	$\boldsymbol{w}$
Nitrogen	28.0134	126.26	3.4	0.0039
Halon 1301	148.93	340.15	3.97	0.0171

Table B.5: Properties of nitrogen and Halon 1301

Next, a value for liquid Halon mole fraction is chosen, $\mathcal{X}_h$, and multicomponent parameters corresponding to the liquid are computed. With respect to the binary interaction parameters, a correlation has been proposed from three discrete values [7], even though it is only valid for temperature values ranging from 293.15 K to 313.15 K. Consequently, it has been decided to consider $k_{ij} = 0.05$, $i \neq j$.

Once all fixed parameters are computed, the iterative process starts.

1. A value for the pressure is chosen, p_1, and the coefficients of the cubic equation are obtained. As $\hat{f}_k^{\epsilon} = \hat{f}_k^{\epsilon}(\mathcal{X}_k, p, T)$, temperature but also liquid composition $\mathcal{X}_k$ do not vary in each iteration.
2. Vapor composition is computed, $\mathcal{Y}_k = K_k \mathcal{X}_k$, where K_k is the equilibrium constant of the specie k. The value corresponding to the first iteration is approximated by means of Wilson equation [33]. As vapor composition is known, it is possible to compute the multicomponent parameters corresponding to the liquid.
3. Liquid and vapor compressibility factors are obtained by solving the corresponding cubic equations. It is important to remark that the roots of each equation can be one real and two complex conjugate or three reals. In the first case the choice is immediate, while in the second one it has to be taken into account that the root with higher value is related to the vapor, the intermediate represents an unstable state and the lower one is related to the liquid.

4. Fugacity coefficients of both phases are computed. Moreover, as $\hat{f}_k^l = \mathcal{X}_k \hat{\phi}_k^l p$ and $\hat{f}_k^v = \mathcal{Y}_k \hat{\phi}_k^v p$, fugacities of both phases can be directly obtained.
5. It has to be checked if (B.1) is verified or not. This can be numerically expressed as follows:

$$\sum_{k=1}^{n} \left(1 - \frac{\hat{f}_k^l}{\hat{f}_k^v} \right) < \varepsilon, \tag{B.7}$$

where $\varepsilon \simeq 10^{-12}$. If the condition (B.7) is fulfilled, equilibrium computation is over and p_1 is the saturation pressure, p_{sat}, while $\mathcal{Y}_k$ is the vapor composition in equilibrium with the liquid of composition $\mathcal{X}_k$.
6. If the value p_1 is not correct, a new value p_2 is chosen. As in equilibrium we have $\hat{f}_k^l = \hat{f}_k^v = \hat{\phi}_k \mathcal{Y}_k p$:

$$\sum_{k=1}^{n} \mathcal{Y}_k = \sum_{k=1}^{n} \frac{\hat{f}_k^{\,l}}{\hat{\phi}_k^v p} = \frac{1}{p} \sum_{k=1}^{n} \frac{\hat{f}_k^{\,l}}{\hat{\phi}_k^v} = 1, \tag{B.8}$$

so pressure can be adjusted as follows:

$$p_{(r+1)} = \left[\sum_{k=1}^{n} \frac{\hat{f}_k^l}{\hat{\phi}_k^v} \right]_{(r)} = p_{(r)} \left[\sum_{k=1}^{n} \frac{\mathcal{X}_k \hat{\phi}_k^l}{\hat{\phi}_k^v} \right]_{(r)} = p_{(r)} \left[\sum_{k=1}^{n} \mathcal{X}_k K_k \right]_{(r)} \tag{B.9}$$

where r is the iteration number and $K_k = \hat{\phi}_k^l / \hat{\phi}_k^v$ is the equilibrium constant, which is modified at each iteration. The number of iterations needed to verify equation (B.7) are done.

To conclude, it is important to note that the results obtained from the present approximation agree with the available experimental data [7, 24, 34].

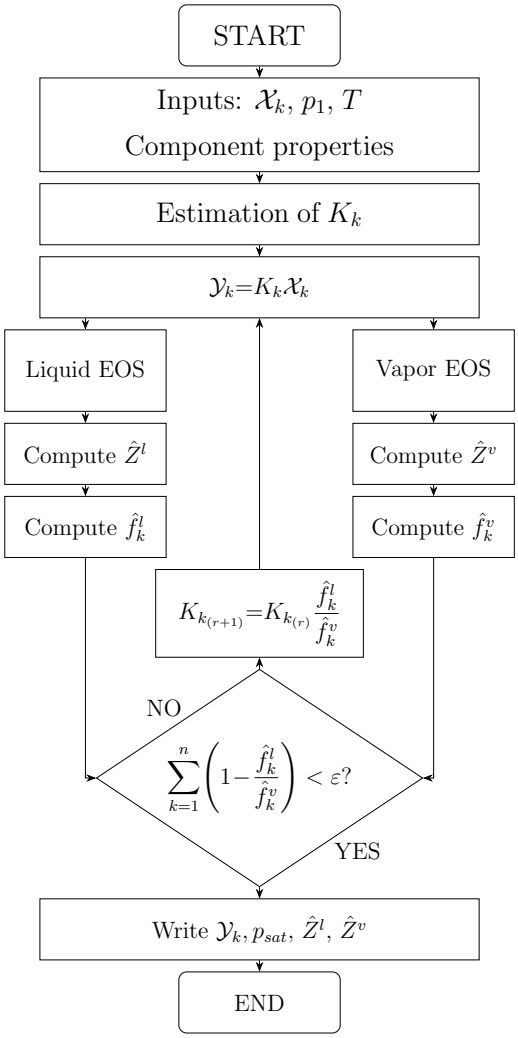

Figure 20: Block diagram of the equilibrium computation function. Adapted from [10]

Appendix B.4. Validity of the model

The accuracy of the proposed model is limited by the critical temperature of the mixture. As Table B.5 shows, Halon 1301 critical temperature $T_{cr_h} =$ 340.15 K, so the code *firex_upm* is not assumed to be valid for temperature values near or above T_{cr_h}.

Furthermore, nitrogen critical temperature $T_{cr_n} = 126.6$ K $< T_{cr_h}$, so the range of validity is reduced if $\mathcal{X}_n$ is increased. In the three considered cases, Figure B.20 shows the existence of a point where the slope of the saturation

pressure changes from positive to negative values. Moreover, when nitrogen is present in the mixture, the curve is characterised by the presence of a discontinuity around the critical point.

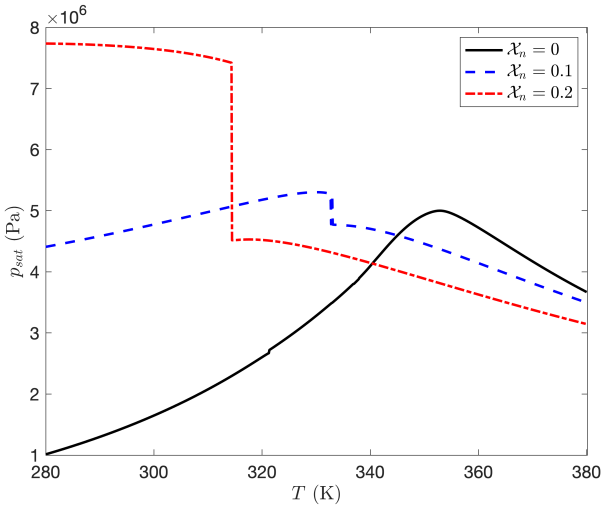

Figure B.20: Saturation pressure of the mixture near the critical temperature

Appendix C. Physical properties

The final appendix deals with the physical properties of the problem. The expressions as a function of temperature are given in Appendix C.1; then, they are validated for certain temperatures by comparing them with the values given by PubChem data repository in Appendix C.2, and, finally, mixture rules are explained in Appendix C.3.

Appendix C.1. Values as a function of temperature near the critical point

The expressions of the transport properties as a function of temperature have been obtained from the ones used in the code *FirEx–BST* [30]. T_{cr_h} is given in Table B.5.

$$c_h = 7.668 \cdot 10^2 - 8.831 \cdot 10^{-1} T_0 + 4.109 \cdot 10^{-3} T_0^2 \quad (\mathrm{J/(kg \cdot K)}) \tag{C.1}$$

$$c_{p_h} = 2.445 \cdot 10^2 + 4.807 \cdot 10^2 \left(\frac{7.284 \cdot 10^2}{T_0 \sinh(7.284 \cdot 10^2 / T_0)} \right)^2 + + 3.069 \cdot 10^2 \left(\frac{3.248 \cdot 10^2}{T_0 \cosh(3.248 \cdot 10^2 / T_0)} \right)^2 \quad (\mathrm{J/(kg \cdot K)}) \tag{C.2}$$

$$c_{p_n} = 1040 \quad (\mathrm{J/(kg \cdot K)}) \tag{C.3}$$

$$c_{v_h} = c_{p_h} - \frac{R}{W_h} \quad (\mathrm{J/(kg \cdot K)}) \tag{C.4}$$

$$c_{v_n} = c_{p_n} - \frac{R}{W_n} \quad (\mathrm{J/(kg \cdot K)}) \tag{C.5}$$

$$L_v = 1.665 \cdot 10^5 \Big(1 - \frac{T_0}{T_{cr_h}} \Big)^{0.353} \quad (\mathrm{J/kg}) \tag{C.6}$$

$$\mu_{h_l} = \exp \Big(-4.671 + \frac{4.783 \cdot 10^2}{T_0} - 9.996 \cdot 10^{-1} \log T_0 \Big) \quad (\mathrm{Pa \cdot s}) \tag{C.7}$$

$$\mu_{h_v} = \frac{1.682 \cdot 10^{-5} T_0^{0.209}}{1 + 7.633 \cdot 10^2 / T_0} \quad (\mathrm{Pa \cdot s}) \tag{C.8}$$

$$\mu_n = 3.098 \cdot 10^{-6} + 4.937 \cdot 10^{-8} T_0 \quad (\mathrm{Pa \cdot s}) \tag{C.9}$$

$$\sigma = 5.453 \cdot 10^{-2} \Big(1 - \frac{T_0}{T_{cr_h}} \Big)^{1.244} \quad (\mathrm{N/m}) \tag{C.10}$$

Appendix C.2. Validation

In this section the values given by the previous expressions are validated. This will be done by taking as a reference the values available at PubChem data repository [26]. All values are taken at $T_0 = 298.15$ K, except from L_v (215.4 K) and μ_n (300.15 K). The units of all parameters are given in the corresponding expression from Appendix C.1, and CP≡ Constant pressure.

Symbol	**Parameter**	**PubChem**	***firex_upm***
c_h	Halon 1301 liquid specific heat	870.272	868.767
c_{p_h}	Halon 1301 vapor specific heat at CP	468.608	465.541
c_{p_h}	Nitrogen specific heat at CP	1040	1040
L_v	Latent heat of vaporization	$1.187 \cdot 10^5$	$1.169 \cdot 10^5$

μ_{h_l}	Halon 1301 liquid viscosity	$1.57 \cdot 10^{-4}$	$1.57 \cdot 10^{-4}$
μ_{h_v}	Halon 1301 vapor viscosity	$1.54 \cdot 10^{-5}$	$1.55 \cdot 10^{-5}$
μ_n	Nitrogen viscosity	$1.79 \cdot 10^{-5}$	$1.79 \cdot 10^{-5}$
σ	Halon 1301 surface tension	0.004	0.004

Table C.6: Validation of physical parameters

Appendix C.3. Mixture rules

A mole-averaged approach is proposed for the multispecies gas; in detail, for the specific heat at constant volume and viscosity, the latter being used in the calculation of the Reynolds number (14):

$$\mu_g = \mathcal{X}_{h_0}\mu_{h_v} + (1 - \mathcal{X}_{h_0})\mu_n; \quad c_v = \mathcal{X}_{h_0}c_{v_h} + (1 - \mathcal{X}_{h_0})c_{v_n}, \tag{C.11}$$

while in the case of the multicomponent mixture, viscosity is volume averaged:

$$\mu_g = \mathcal{X}_{h_0}\mu_{h_l} + (1 - \mathcal{X}_{h_0})\mu_n. \tag{C.12}$$

References

[1] Amatriain, A., Parra, I., and Rubio, G. (2019). Study of Bubble Growth in a Multicomponent Mixture at High Pressure. *Proceedings of the 4th World Congress on Momentum, Heat and Mass Transfer*.

[2] Bein, D. (2006). A Review of the History of Fire Supression on U.S. DOD Aircraft. *Special Publication (NIST SP)*, 984(4).

[3] Braker, W. and Mossman, A. L. (1976). *The Matheson Unabridged Gas Data Book: A Compilation of Physical and Thermodynamic Properties of Gases*. Matheson Company.

[4] Brennen, C. E. (2005). *Fundamentals of Multiphase Flows*. Cambridge University Press.

[5] Burke, R. (2007). *Fire Protection: Systems and Response*. CRC Press.

[6] Butcher, J. C. (2016). *Numerical Methods for Ordinary Differential Equations*. Wiley.

[7] Chen, M., Xie, Y., Wu, H., Shi, S., and Yu, J. (2017). Modeling Solubility of Nitrogen in Clean Fire Extinguishing Agent by Peng-Robinson Equation of State and a Correlation of Henry's Law Constants. *Applied Thermal Engineering*, 110:457–468.

[8] Colebrook, C. F. (1939). Turbulent Flow in Pipes, with Particular Reference to the Transition Region Between the Smooth and Rough Pipe Laws. *Journal of the Institution of Civil Engineers*, 11(4):133–156.

[9] Coward, R. N., Hillaert, J. A., and McCrory, D. M. (1992). Analytical Methods for Modeling Discharge Characteristics of Halon 1301 Fire Protection Systems. *National Institute of Standards and Technology*.

[10] Danesh, A. (1998). *PVT and Phase Behaviour of Petroleum Reservoir Fluids*. Elsevier Science & Technology Books.

[11] Darcy, H. (1857). Recherches Expérimentales Relatives au Mouvement de l'Eau Dans les Tuyaux. *Imprimerie Nationale*.

[12] Deligiannis, P. and Cleaver, J. W. (1992). Determination of the Heterogeneous Nucleation Factor During a Transient Liquid Expansion. *International Journal of Multiphase Flow*, 18(2):273–278.

[13] Denbigh, K. (1981). *The Principles of Chemical Equilibrium: With Applications in Chemistry and Chemical Engineering*. Cambridge University Press, 4th edition.

[14] Development Team, R. (1995). RELAP5/MOD3.2 Code Manuals. *U. S. Nuclear Regulatory Commission Report NUREG/CR-5535*.

[15] Elliott, D. G., Garrison, P. W., Klein, G. A., Moran, K. M., and Zydowicz, M. P. (1984). Flow of Nitrogen-Pressurized Halon 1301 in Fire Extinguishing Systems. *JPL Publication*, 84(62).

[16] European Union Aviation Safety Agency (2019). Halon Replacement in the Aviation Industry.

[17] Fabian, P. and Singh, O. N. (1999). *Reactive Halogen Compounds in the Atmosphere*. Springer.

[18] Forsythe, G., Malcolm, M., and Moler, C. (1977). *Computer Methods for Mathematical Computations*. Prentice Hall.

[19] Gallagher, J., McLinden, M., Morrison, G., and Huber, M. (1993). NIST Thermodynamic Properties of Refrigerants and Refrigerant Mixtures Database (REFPROP). *U. S. Nuclear Regulatory Commission Report NUREG/CR-5535*.

[20] Gustafsson, B., Kreiss, H. O., and Oliger, J. (2013). *Time-Dependent Problems and Difference Methods*. Wiley.

[21] Jin, J., An, F., Shou, Y., Pan, R., Xuan, Y., and Li, Q. (2018). Simulation on Release Characteristics of the Gas Extinguishing Agent in Fire Extinguisher Vessel with Different Filling Conditions Based on AMESim. *Procedia Engineering*, 211:315–324.

[22] Kim, J., Baek, B., and Lee, J. (2009). Numerical Analysis of Flow Characteristics of Fire Extinguishing Agents in Aircraft Fire Extinguishing Systems. *Journal of Mechanical Science and Technology*, 23:1877–1884.

[23] Landau, L. D. and Lifshitz, E. M. (1987). *Fluid Mechanics: Volume 6 (Course of Theoretical Physics)*. Butterworth-Heinemann, 2nd edition.

[24] Lim, J. S. and Kim, J. D. (1997). Vapor-Liquid Equilibria of the Binary Systems Nitrogen + Bromotrifluoromethane, + Bromochlorodifluoromethane, + 1,1,1,2,3,3,3-Heptafluoropropane, and + Trifluoroiodomethane from 293.2 to 313.2 k and 30 to 100 bar. *Journal of Chemical Engineering*, 42:112–115.

[25] Mcbee, E. et al. (1947). Final Report on Fire-Extinguishing Agents. *Department of Chemistry - Purdue University*.

[26] National Center for Biotechnology Information (2020). PubChem Data Repository. `https://pubchem.ncbi.nlm.nih.gov`.

[27] Peng, D. Y. and Robinson, D. B. (1976). A New Two-Constant Equation of State. *Industrial and Engineering Chemistry Fundamentals*, 15(1):59–64.

[28] Picard, D. J. and Bishnoi, P. R. (1987). Calculation of the Thermodynamic Sound Velocity in Two-Phase Multicomponent Fluids. *International Journal of Multiphase Flow*, 13(3):295–308.

[29] Powell, M. J. D. (1968). A Fortran Subroutine for Solving Systems of Nonlinear Algebraic Equations. *Atomic Energy Research Establishment*.

[30] Snegirev, A. and Lipjainen, A. (2010). Numerical Modeling and Experimental Studies of Discharge and Spread of Two-Phase Gas-Droplet Fire Extinguishing Agent. *Saint-Petesburg State Polytechnic University*.

[31] Trapp, J. A. and Ransom, H. (1982). A Choked-Flow Calculation Criterion for Nonhomogeneous, Nonequilibrium, Two-Phase Flows. *International Journal of Multiphase Flow*.

[32] Tuzla, K., Palmer, T., Chen, J. C., Sundaram, R. K., and Yeung, W. S. (2000). Development of Computer Program for Fire Supressant Fluid Flow. *Lehigh University & Duke Engineering and Services, Inc.*

[33] Wilson, G. A. (1968). A Modified Redlich-Kwong EOS. Application to Physical Data Calculation. *Annual Meeting of Chemical Engineers*, 150.

[34] Yang, J. C., Vázquez, I., Boyer, C. I., Huber, M. L., and Weber, L. (1997). Measured and Predicted Thermodynamic Properties of Selected Halon Alternative/Nitrogen Mixtures. *International Journal of Refrigeration*, 20(2):96–105.

[35] Zou, Y., Vahdat, N., and Collins, M. M. (2001). Fire Supression Efficiency of Bromoalkene/Nitrogen Gas Mixtures as Totagflooding Agents. *Halon Options Technical Working Conference*, pages 306–313.